because of nonachievement of transient equilibrium had much effect on the graphical analysis as compared with BP_{ND}. Therefore, we estimated B_{max} and K_d by the graphical analysis with the relationship between BP_{ND} and B^{ref}.

In the simulations with various injected masses of [^{11}C]raclopride, it was shown that the relationship between BP_{ND} and B^{ref} became linear to some extent. However, BP_{ND} deviated from the linear relationship and approached a nonzero value when B^{ref} became larger (Figure 2). Therefore, in the B_{max} and K_d estimation by the graphical analysis with the reference TAC, points must be plotted within the range of the linear relation. As the relationship between BP_{ND} and B estimated from C_b using the plasma input function, without the reference TAC, remained linear even when B became large and the estimated BP_{ND} approached 0 (data not shown), this apparent saturation seemed to be owing to the reference region. Strictly speaking, the time course of free radioligand C_f is different from that of the reference region C_r (Figure 1) and C_f changes according to the specific binding that was affected by k_{on}, B_{max}, or administered mass of raclopride as pointed out by Ito *et al* (1998). Therefore, the time of the transient equilibrium estimated using C_b^{ref} was different from that estimated using C_b, and B^{ref} was often different as well. In addition, the value of BP_{ND} estimated by SRTM was lower than the BP_{ND} estimated from the two-tissue compartment model with the plasma input function.

This difference between the target and reference TAC affected the B_{max} and K_d estimates as well. In the simulated TACs with various B_{max} or K_d values, the B_{max} and K_d were overestimated compared with the true values even in the conventional three PET scan approach (Figure 3). On the other hand, the overestimation was not observed when B_{max} and K_d were estimated by the graphical analysis using C_f and C_b without the reference TAC (Figure 3), demonstrating that graphical analysis could determine B_{max} and K_d precisely if C_b were obtained correctly. However, the free and bound concentrations in the target region cannot be distinguished from the total concentration measured by PET scanning without arterial blood sampling, and in practical PET data, estimation of rate constants with the plasma input function is unstable and impractical. Therefore, in the usual graphical analysis, the TAC of reference region is used as the free radioligand concentration in the target region (Farde *et al*, 1989). The effect of the reference TAC on B_{max} and K_d estimates depends on the kinetics of the tracer in each region, which depends in turn on the particular tracers and species. In the simulated TACs of monkeys with [^{11}C]raclopride, there was a good correlation between true and estimated K_d or B_{max}, though estimates were biased. Therefore, we concluded the graphical analysis with reference TAC is practical for [^{11}C]raclopride studies, because it can detect the value of B_{max} or K_d in neurological or psychiatric disorders without arterial blood sampling.

Estimated Density and Affinity by the Multiple-Injection Approach

We applied the multiple-injection approach to the graphical analysis for B_{max} and K_d determination in an effort to shorten the total duration of the scanning protocol, and to obviate the need for several radiosyntheses for each animal. From the relationship between the BP_{ND} estimates and injected mass in the simulation study (Figure 2), the molar amounts of three injections were set as 1.5, 10, and 30 nmol/kg, so that the estimated BP_{ND} would be high, intermediate, and low within the range in which the linear correlation held. The injection interval was set to 50 mins, because it has been reported in monkey studies that 50 mins scan duration could provide reliable BP_{ND} estimates even for TACs with high and low BP_{ND} values (Ikoma *et al*, 2009). In our present studies on monkeys with this protocol, injected masses increased with each successive injection, but amounts of administered radioactivity remained fairly constant, i.e., 57, 60, and 31 MBq. Therefore, the signal to noise ratio of image quality did not change seriously for each injection.

In the usual graphical analysis by nonsequential multiple PET scans, the molar amount of administered [^{11}C]raclopride for each scan is adjusted by varying the specific activity of administered [^{11}C] raclopride. Several investigators have attempted to perform multiple injections of ligands with PET studies to obtain receptor density and affinity by changing specific activity with a detailed model equation (Delforge *et al*, 1995; Millet *et al*, 1995; Morris *et al*, 1996; Muzic *et al*, 1996; Christian *et al*, 2004; Gallezot *et al*, 2008). Meanwhile, our approach requires only one synthesis of [^{11}C]raclopride, which is split to three with different mass of raclopride with same specific activity. By keeping the specific activity throughout scan, we can directly interpret PET counts in pmol/mL unit.

In the simulations of B_{max} and K_d estimation with this single PET scan approach, B_{max} and K_d were overestimated compared with the true values, just as seen in the three PET scan approach. Furthermore, estimates of both parameters were higher than those in the three PET scan approach. In the single PET scan approach, the error because of assumptions of the reference tissue approach could be more severe than for the three PET scan approach, because the residual radioactivities at the times of the second and third injections could propagate to error of B^{ref} or BP_{ND} estimates. This was shown to be the case in the simulation study, in which the relationship between the BP_{ND} and B^{ref} in the third injection was a little different from that in the first injection (Figure 2). Furthermore, our approach assumes that BP_{ND} is promptly altered by the next injection, but this is in fact not exactly the case. We showed the bias of the estimated BP_{ND} related to this assumption (Ikoma *et al*, 2009), and the estimated B_{max} and K_d in this paper consequently could be biased. However, in the

simulations, B_{max} and K_d estimated by the MI-GA changed according to the variation of the true values (Figure 3), demonstrating this approach could be applied to the quantitative evaluation of B_{max} and K_d from a single session of PET scanning.

Monkey Studies

In the simulations, we demonstrated that the MI-GA could detect density and affinity of dopamine D_2 receptors. Furthermore, we demonstrated the validity of the proposed method using actual data from monkeys. As a result, the three BP_{ND} data points calculated from the single PET scan with three sequential injections of different administration masses were almost on a straight line, and estimated values of B_{max} and K_d were very close to those previously obtained *in vitro* ($B_{max} = 25.7$ pmol/g) (Madras *et al*, 1988) or *in vivo* by the conventional method in monkeys ($B_{max} = 22$ pmol/mL, $K_d = 13.5$ nmol/L) (Doudet *et al*, 2003). The estimates by the single PET scan approach were slightly higher than those by the three PET scan approach, and this was consistent with the results from the current simulations.

Although we investigated only three monkeys in this study, the values of B_{max} in the partially denervated striata was higher than in normal striatum, whereas the apparent affinity was unaffected by the MPTP lesions. Likewise Rinne *et al* (1995) reported a 35% increase in the D_2 B_{max} in the putamen contralateral to the side of predominant motor symptoms, without any discernible effect on apparent affinity. In our monkey measurements, in the hemilesioned monkey, the B_{max} was elevated by 31% on the denervated side. In the animal with bilateral MPTP lesion, the B_{max} in both striata was higher than in the normal animal, or in the unlesioned side of the hemiparkinsonian animal, despite no significant changes in K_d values: the results were consistent with those of the previous report.

In addition to the results of ROI analysis, which disclosed bulk D_2 receptor characteristics in the whole striatum, parametric imaging of B_{max} and K_d (as shown in Figure 5) suggested a potential significance in regional estimation of D_2 receptor characteristics. Although ROI analysis disclosed higher B_{max} values in the MPTP-infused side of the striatum, the parametric imaging showed the increase of B_{max} was more evident in the dorsal and posterior parts of the striatum. A similar finding of preferential lesion in dorsal and posterior parts of the striatum has been reported based on neurochemical and pathological assessments of MPTP-lesioned monkeys (Oiwa *et al*, 2003). As the current parametric imaging may have significant artifacts, such as those arising from low signal-to-noise ratio, partial volume effects, small number of points, the situation should be improved through the use of a higher resolution PET scanner.

Potential Limitations of the Multiple-Injection Graphical Analysis

The multiple-injection approach is able to assess the B_{max} and K_d for receptor studies in a single PET scan with single radiosynthesis, and shortened study period as compared with a conventional approach. This approach might also be applicable to other PET ligands and receptor types, but with several caveats: First, it is necessary to evaluate whether the reference region can be used as the free TAC of the target region. The kinetics of the target and reference regions is affected by the value of each rate constant, i.e., K_1, k_2, B_{max}, and K_d, that differ between species and radioligands. The difference between C_{ref} and C_f often causes an error in B^{ref}, and the estimated B_{max} and K_d should be interpreted with caution when the reference region has considerably different kinetics. Second, the molar amounts of administered ligand need to be selected such that the resultant BP_{ND} will be within the range in which the linear relationship between BP_{ND} and B holds. In the case of regions with low BP_{ND}, and small extent of the necessary linear relationship, it may be difficult to determine B_{max} and K_d reliably. Third, the interval of three injections should be determined so that the free ligand TAC has a transient equilibrium within the scan duration of each injection, especially when the injected mass is small, i.e., BP_{ND} is high. The radioligand [^{11}C]raclopride dissociates rapidly from the receptors, allowing equilibration of binding to be established *in vivo* within the time span of PET experiments (Farde *et al*, 1989; Ito *et al*, 1998). However, those ligands with slow kinetics, such as [^{18}F]fallypride require a longer scan duration such that the present graphical analysis may not be suitable in all instances. Despite these limitations, by optimizing the administered mass and the time interval between three injections of [^{11}C]raclopride, we have shown that the multiple-injection approach can determine B_{max} and K_d values as effectively as an approach using three separate scans, but within a single scan time of 150 mins.

Moreover, the bias of B_{max} and K_d estimated by the single scan approach with two injections was not larger than that by the single scan approach with three injections in the simulations (data not shown), and points of the second and third injections in MI-GA were almost on the same line in the monkey studies (Figure 6). Therefore, there is a possibility of reducing scan time and exposure further using only two injections, though the effect of statistical noise on estimates should be considered.

Conclusion

We developed the method for estimating B_{max} and K_d values in a single session of PET scanning with multiple injections of [^{11}C]raclopride. Our simulations showed that the MI-GA could detect B_{max} and K_d values by using the optimal injection protocol. We

also demonstrated in monkey studies that B_{max} and K_d values estimated by our proposed approach were proper compared with previous monkey studies or our studies by the conventional method. The proposed method made it possible to determine the dopamine D_2 receptor density and affinity by a 150 mins PET scan with three injections of [^{11}C]raclopride at 50 mins intervals.

Acknowledgements

We thank Dr Jun Takahashi (Kyoto University) for providing us animals for this study. This research was supported by the Ministry of Education, Culture, Sports, Science and Technology of Japan (MEXT) grant-in-aid for Young Scientists (B) (No. 20790839), grant-in-aid for Scientific Research (C) (No. 09019855) (TH), Kobe Cluster I and II, and the Ministry of Health, Labour, and Welfare of Japan (MHLW) Health Science Research Grant, H17-025 (TH, HI). We are grateful to members of Department of Investigative Radiology, National Cardiovascular Center Research Institute, for their support of PET experiment and for helpful suggestions.

Conflict of interest

The authors declare no conflict of interest.

References

Bankiewicz KS, Oldfield EH, Chiueh CC, Doppman JL, Jacobowitz DM, Kopin IJ (1986) Hemiparkinsonism in monkeys after unilateral internal carotid artery infusion of 1-methyl-4-phenyl-1,2,3,6-tetrahydropyridine (MPTP). *Life Sci* 39:7–16

Christian BT, Narayanan T, Shi B, Morris ED, Mantil J, Mukherjee J (2004) Measuring the *in vivo* binding parameters of [^{18}F]-fallypride in monkeys using a PET multiple-injection protocol. *J Cereb Blood Flow Metab* 24:309–22

Cross AJ, Crow TJ, Owen F (1981) ^{3}H-Flupenthixol binding in post-mortem brains of schizophrenics: evidence for a selective increase in dopamine D2 receptors. *Psychopharmacology (Berl)* 74:122–4

Delforge J, Pappata S, Millet P, Samson Y, Bendriem B, Jobert A, Crouzel C, Syrota A (1995) Quantification of benzodiazepine receptors in human brain using PET, [^{11}C]flumazenil, and a single-experiment protocol. *J Cereb Blood Flow Metab* 15:284–300

Doudet DJ, Holden JE (2003) Sequential versus non-sequential measurement of density and affinity of dopamine D_2 receptors with [^{11}C]raclopride: Effect of methamphetamine. *J Cereb Blood Flow Metab* 23:1489–94

Doudet DJ, Jivan S, Holden JE (2003) *In vivo* measurement of receptor density and affinity: comparison of the routine sequential method with a nonsequential method in studies of dopamine D_2 receptors with [^{11}C]raclopride. *J Cereb Blood Flow Metab* 23:280–4

Farde L, Ehrin E, Eriksson L, Greitz T, Hall H, Hedström CG, Litton JE, Sedvall G (1985) Substituted benzamides as ligands for visualization of dopamine receptor binding in the human brain by positron emission tomography. *Proc Natl Acad Sci USA* 82:3863–7

Farde L, Eriksson L, Blomquist G, Halldin C (1989) Kinetic analysis of central [^{11}C]raclopride binding to D_2-dopamine receptors studied by PET — A comparison to equilibrium analysis. *J Cereb Blood Flow Metab* 9: 696–708

Farde L, Hall H, Ehrin E, Sedvall G (1986) Quantitative analysis of D_2 dopamine receptor binding in the living human brain by PET. *Science* 231:258–61

Farde L, Wiesel FA, Hall H, Halldin C, Stone-Elander S, Sedvall G (1987) No D_2 receptor increase in PET study of schizophrenia. *Arch Gen Psychiatry* 44:671–2

Farde L, Wiesel FA, Stone-Elander S, Halldin C, Nordström AL, Hall H, Sedvall G (1990) D_2 dopamine receptors in neuroleptic-naive schizophrenic patients. A positron emission tomography study with [^{11}C]raclopride. *Arch Gen Psychiatry* 47:213–9

Gallezot JD, Bottlaender MA, Delforge J, Valette H, Saba W, Dollé F, Coulon CM, Ottaviani MP, Hinnen F, Syrota A, Grégoire MC (2008) Quantification of cerebral nicotinic acetylcholine receptors by PET using 2-[^{18}F]fluoro-A-85380 and the multiinjection approach. *J Cereb Blood Flow Metab* 28:172–89

Gunn RN, Lammertsma AA, Hume SP, Cunningham VJ (1997) Parametric imaging of ligand-receptor binding in PET using a simplified reference region model. *Neuroimage* 6:279–87

Guttman M, Seeman P (1985) L-dopa reverses the elevated density of D_2 dopamine receptors in Parkinson's diseased striatum. *J Neural Transm* 64:93–103

Hall H, Köhler C, Gawell L, Farde L, Sedvall G (1988) Raclopride, a new selective ligand for the dopamine-D_2 receptors. *Prog Neuropsychopharmacol Biol Psychiatry* 12:559–68

Herzog H, Tellmann L, Hocke C, Pietrzyk U, Casey ME, Kuwert T (2004) NEMA NU2-2001 guided performance evaluation of four Siemens ECAT PET scanners. *IEEE Trans Nucl Science* 51:2662–9

Ikoma Y, Watabe H, Hayashi T, Miyake Y, Teramoto N, Minato K, Iida H (2009) Quantitative evaluation of changes in binding potential with a simplified reference tissue model and multiple injections of [^{11}C]raclopride. *Neuroimage* 47:1639–48

Ito H, Hietala J, Blomqvist G, Halldin C, Farde L (1998) Comparison of the transient equilibrium and continuous infusion method for quantitative PET analysis of [^{11}C]raclopride binding. *J Cereb Blood Flow Metab* 18:941–50

Joyce JN, Lexow N, Bird E, Winokur A (1988) Organization of dopamine D_1 and D_2 receptors in human striatum: receptor autoradiographic studies in Huntington's disease and schizophrenia. *Synapse* 2:546–57

Köhler C, Hall H, Ogren SO, Gawell L (1985) Specific *in vitro* and *in vivo* binding of ^{3}H-raclopride. A potent substituted benzamide drug with high affinity for dopamine D-2 receptors in the rat brain. *Biochem Pharmacol* 34:2251–9

Lammertsma AA, Hume SP (1996) Simplified reference tissue model for PET receptor studies. *Neuroimage* 4:153–8

Logan J, Fowler JS, Volkow ND, Wang GJ, Ding YS, Alexoff DL (1996) Distribution volume ratios without blood sampling from graphical analysis of PET data. *J Cereb Blood Flow Metab* 16:834–40

Logan J, Volkow ND, Fowler JS, Wang GJ, Fischman MW, Foltin RW, Abumard NN, Vitkun S, Gatley SJ, Pappas N, Hitzemann R, Shea CE (1997) Concentration and occupancy of dopamine transporters in cocaine abusers with [^{11}C]cocaine and PET. *Synapse* 27:347–56

Madras BK, Fahey MA, Canfield DR, Spealman RD (1988) D1 and D2 dopamine receptors in caudate-putamen of nonhuman primates (*macaca fascicularis*). *J Neurochem* 51:934–43

Millet P, Delforge J, Mauguiere F, Pappata S, Cinotti L, Frouin V, Samson Y, Bendriem B, Syrota A (1995) Parameter and index images of benzodiazepine receptor concentration in the brain. *J Nucl Med* 36:1462–71

Mintun MA, Raichle ME, Kilbourn MR, Wooten GF, Welch MJ (1984) A Quantitative model for the *in vivo* assessment of drug binding sites with positron emission tomography. *Ann Neurol* 15:217–27

Morris ED, Babich JW, Alpert NM, Bonab AA, Livni E, Weise S, Hsu H, Christian BT, Madras BK, Fischman AJ (1996) Quantification of dopamine transporter density in monkeys by dynamic PET imaging of multiple injections of ^{11}C-CFT. *Synapse* 24:262–72

Muzic RR, Nelson AD, Saidel GM, Miraldi F (1996) Optimal experiment design for PET quantification of receptor concentration. *IEEE Trans Med Imaging* 15:2–12

Oiwa Y, Eberling JL, Nagy D, Pivirotto P, Emborg ME, Bankiewicz KS (2003) Overlesioned hemiparkinsonian non human primate model: correlation between clinical, neurochemical and histochemical changes. *Front Biosci* 8:155–66

Rinne JO, Laihinen A, Ruottinen H, Ruotsalainen U, Någren K, Lehikoinen P, Oikonen V, Rinne UK (1995) Increased density of dopamine D_2 receptors in the putamen, but not in the caudate nucleus in early Parkinson's disease: a PET study with [^{11}C]raclopride. *J Neurol Sci* 132:156–61

Scatchard G (1949) The attractions of proteins for small molecules and ions. *Ann NY Acad Sci* 51:660–72

Seeman P, Bzowej NH, Guan HC, Bergeron C, Reynolds GP, Bird ED, Riederer P, Jellinger K, Tourtellotte WW (1987) Human brain D_1 and D_2 dopamine receptors in schizophrenia, Alzheimer's, Parkinson's, and Huntington's diseases. *Neuropsychopharmacology* 1:5–15

Takagi Y, Takahashi J, Saiki H, Morizane A, Hayashi T, Kishi Y, Fukuda H, Okamoto Y, Koyanagi M, Ideguchi M, Hayashi H, Imazato T, Kawasaki H, Suemori H, Omachi S, Iida H, Itoh N, Nakatsuji N, Sasai Y, Hashimoto N (2005) Dopaminergic neurons generated from monkey embryonic stem cells function in a Parkinson primate model. *J Clin Invest* 115:102–9

Watabe H, Ohta Y, Teramoto N, Miyake Y, Kurokawa M, Yamamoto A, Ose Y, Hayashi T, Iida H (2006) A novel reference tissue approach for multiple injections of [C-11]Raclopride. *Neuroimage* 31:T73

Wong DF, Wagner Jr HN, Tune LE, Dannals RF, Pearlson GD, Links JM, Tamminga CA, Broussolle EP, Ravert HT, Wilson AA, Toung JK, Malat J, Williams JA, O'Tuama LA, Snyder SH, Kuhar MJ, Gjedde A (1986) Positron emission tomography reveals elevated D_2 dopamine receptors in drug-naive schizophrenics. *Science* 234:1558–63

Appendix

The multiple-injection two-tissue four-parameter compartment model is based on the following differential equations:

$$\frac{dC_f}{dt} = K_1 C_p(t) - (k_2 + k_3) C_f(t) + k_4 C_b(t) \qquad \text{(A1)}$$

$$\frac{dC_b}{dt} = k_3 C_f(t) - k_4 C_b(t) \qquad \text{(A2)}$$

where C_p is the radioactivity concentration of metabolite-corrected plasma, C_f and C_b are the concentrations of radioactivity for free and specifically bound ligand in tissue, respectively.

Equations (A1) and (A2) are solved with the radioactivity concentration of C_f and C_b at the time of injection, that is $C_f(0)$ and $C_b(0)$, then $C_f(t)$, $C_b(t)$ and total radioactivity concentration in tissue $C_t(t)$ are expressed as following equations:

$$\begin{aligned} C_f(t) =& \frac{K_1}{\alpha_2 - \alpha_1}\{(k_4 - \alpha_1)e^{-\alpha_1 t} - (k_4 - \alpha_2)e^{-\alpha_2 t}\} \otimes C_p(t) \\ &+ \frac{1}{\alpha_2 - \alpha_1}\{(k_4 - \alpha_1)C_f(0) + k_4 C_b(0)\}e^{-\alpha_1 t} \\ &- \frac{1}{\alpha_2 - \alpha_1}\{(k_4 - \alpha_2)C_f(0) + k_4 C_b(0)\}e^{-\alpha_2 t} \end{aligned} \qquad \text{(A3)}$$

$$\begin{aligned} C_b(t) =& \frac{K_1 k_3}{\alpha_2 - \alpha_1}\left(e^{-\alpha_1 t} - e^{-\alpha_2 t}\right) \\ &\otimes C_p(t) + \frac{k_3}{\alpha_2 - \alpha_1}\left(C_f(0) + \frac{k_4}{k_4 - \alpha_1} C_b(0)\right)e^{-\alpha_1 t} \\ &- \frac{k_3}{\alpha_2 - \alpha_1}\left(C_f(0) + \frac{k_4}{k_4 - \alpha_2} C_b(0)\right)e^{-\alpha_2 t} \\ &+ \left(\frac{k_3 k_4}{(k_4 - \alpha_1)(k_4 - \alpha_2)} + 1\right) C_b(0) e^{-k_4 t} \end{aligned} \qquad \text{(A4)}$$

$$\begin{aligned} C_t(t) =& \frac{K_1}{\alpha_2 - \alpha_1}\{(k_3 + k_4 - \alpha_1)e^{-\alpha_1 t} - (k_3 + k_4 - \alpha_2)e^{-\alpha_2 t}\} \\ &\otimes C_p(t) + \frac{k_3 + k_4 - \alpha_1}{\alpha_2 - \alpha_1}\left(C_f(0) + \frac{k_4}{k_4 - \alpha_1} C_b(0)\right)e^{-\alpha_1 t} \\ &- \frac{k_3 + k_4 - \alpha_2}{\alpha_2 - \alpha_1}\left(C_f(0) + \frac{k_4}{k_4 - \alpha_2} C_b(0)\right)e^{-\alpha_2 t} \\ &+ \left(\frac{k_3 k_4}{(k_4 - \alpha_1)(k_4 - \alpha_2)} + 1\right) C_b(0) e^{-k_4 t} \\ \alpha_{1,2} =& \frac{(k_2 + k_3 + k_4) \mp \sqrt{(k_2 + k_3 + k_4)^2 - 4k_2 k_4}}{2} \end{aligned} \qquad \text{(A5)}$$

Ann Nucl Med (2010) 24:413–420
DOI 10.1007/s12149-010-0374-x

ORIGINAL ARTICLE

Optimization of transmission scan duration for ^{15}O PET study with sequential dual tracer administration using *N*-index

Nobuyuki Kudomi · Hiroshi Watabe · Takuya Hayashi · Hisashi Oka · Yoshinori Miyake · Hidehiro Iida

Received: 14 October 2009 / Accepted: 4 March 2010 / Published online: 17 April 2010

Abstract
Purpose Cerebral blood flow (CBF), oxygen extraction fraction (OEF) and cerebral metabolic rate of O_2 ($CMRO_2$) can be quantified by PET with the administration of $H_2^{15}O$ and $^{15}O_2$. Recently, a shortening in the duration of these measurements was achieved by the sequential administration of dual tracers of $^{15}O_2$ and $H_2^{15}O$ with PET acquisition and integration method (DARG method). A transmission scan is generally required for correcting photon attenuation in advance of PET scan. Although the DARG method can shorten the total study duration to around 30 min, the transmission scan duration has not been optimized and has possibility to shorten its duration. Our aim of this study was to determine the optimal duration for the transmission scan. We introduced '*N*-index', which estimates the noise level on an image obtained by subtracting two statistically independent and physiologically equivalent images. The relationship between noise on functional images and duration of the transmission scan was investigated by *N*-index.
Methods We performed phantom studies to test whether the *N*-index reflects the pixel noise in a PET image. We also estimated the noise level by the *N*-index on CBF, OEF and $CMRO_2$ images from DARG method in clinical patients, and investigated an optimal true count of the transmission scan.
Results We found tight correlation between pixel noise and *N*-index in the phantom study. By investigating relationship between the transmission scan duration and *N*-index value for the functional images by DARG method, we revealed that the transmission data with true counts of more than 40 Mcounts results in CBF, OEF, and $CMRO_2$ images of reasonable quantitative accuracy and quality.
Conclusion The present study suggests that further shortening of DARG measurement is possible by abridging the transmission scan. The *N*-index could be used to determine the optimal measurement condition when examining the quality of image.

Keywords Transmission scan · PET · O-15 gas · Image quality

N. Kudomi
Department of Medical Physics, Faculty of Medicine, Kagawa University, Mikichou, Kitagun, Kagawa 761-0793, Japan

H. Watabe (✉)
Department of Molecular Imaging in Medicine, Osaka University Graduate School of Medicine, 2-2 Yamadaoka, Suita, Osaka 565-0871, Japan
e-mail: watabe@mi.med.osaka-u.ac.jp

N. Kudomi · H. Watabe · T. Hayashi · H. Iida
Department of Investigative Radiology, Advanced Medical-Engineering Center, National Cardiovascular Center-Research Institute, 5-7-1, Fujishirodai, Suita, Osaka 565-8565, Japan

H. Oka · Y. Miyake
Department of Radiology, National Cardiovascular Center, Hospital, 5-7-1, Fujishirodai, Suita, Osaka 565-8565, Japan

Introduction

Cerebral blood flow (CBF), oxygen extraction fraction (OEF) and cerebral metabolic rate of oxygen ($CMRO_2$) images have facilitated the understanding of the pathophysiological basis of cerebro-vascular disorders, and these images can be quantitatively measured using positron emission tomography (PET) with bolus administrations of ^{15}O-labeled oxygen ($^{15}O_2$) and water ($H_2^{15}O$) [1]. In the conventional three-step method [1–3], these functional

images were measured with separate scans for three tracers of $C^{15}O$ for cerebral blood volume (CBV), $H_2^{15}O$ for CBF and $^{15}O_2$ for $CMRO_2$, and there were additional waiting times between the scans in order to avoid the contamination of the previous tracer on the PET data. Therefore, the measurement process required a relatively long duration of around 1 h in the conventional method. Recently, the duration of the CBF, OEF and $CMRO_2$ measurements was shortened using a dual tracer autoradiography (DARG) method [4]. The DARG method is characterized by sequentially administrating dual tracers of $^{15}O_2$ and $H_2^{15}O$ typically for 3 min interval during a single PET scan. When compared with the conventional three-step method, the DARG method can shorten the total study period to approximately 30 min for the set of CBV, CBF, OEF and $CMRO_2$ measurements while maintaining the image quality and quantitative accuracy.

In order to shorten the examination period even more, one option is to eliminate the CO scan which is used to correct for radioactivity in vascular space [5]. The other is to shorten the duration of the transmission scan, which is required to correct the attenuation of the number of pairs of emitted 511 keV photons in the materials of brain or other, to quantitatively estimate the radio-tracer concentrations. Usually, transmission scan is performed with external ^{68}Ge sources [6, 7]. By prolonging the duration of transmission scan, the accuracy of attenuation correction (AC) will be improved, which results in better quality and accuracy of the functional images although a patient receives additional radiation exposures. In contrast, by shortening the duration of the transmission scan, the functional images might be deteriorated due to lack of statistics. Thus, optimization of transmission scan duration is needed. Because the ^{68}Ge rod sources radioactively decay with a half-life of 270.95 days, the optimal transmission scan duration depends on the radioactivity of the ^{68}Ge source and should be determined by the true transmission scan count. To determine the optimal true count of the transmission scan, quantitative accuracy (bias) and image quality (noise on image) of the CBF, OEF and $CMRO_2$ images must be considered. The quantitative accuracy can be evaluated by comparing two images generated from different transmission scan durations. Noise equivalent counts, NEC, is often used index to evaluate noise in PET image. However, by the NEC, noise propagation from the transmission scan cannot be assessed. Alternatively, to determine the quality of images, one can perform replicated PET measurements and evaluate pixel-wise standard deviation (SD) from these images [8]. Acquiring multiple images, however, are not practical, because measurement conditions such as the administration dose and physiological state cannot be equivalent across replicated measurements.

In this study, in order to evaluate image quality, we introduced an '*N*-index' to define the noise level in an image. The validity of the *N*-index was tested using the Hoffman brain phantom [9]. In order to determine the optimal true count for the transmission scan, the introduced *N*-index was used to evaluate the noise level in the CBF, OEF and $CMRO_2$ images obtained from actual PET data with DARG method for patients with cerebro-vascular disease.

Materials and methods

Phantom studies for validation of *N*-index

It has been reported that the pixel-wise SD of a PET image reconstructed by the filtered backward projection (FBP) method was spatially uniform even in a nonhomogenous region [10]. On the basis of this suggestion, if we obtain two images of the same object with same activity concentration level from two independent scans or procedures, a spatial distribution of pixel values in the subtracted image between those two images has zero mean and its variation is related to the noise level of the images. The *N*-index is defined as the SD of the spatial distribution of the subtracted image.

To verify whether the *N*-index can be used as an index for noise level, the computed *N*-index was compared with the pixel-wise SD value of a PET image obtained from scanning a non-uniform object. We performed a PET experiment using the Hoffman brain phantom [9] filled with $^{18}F_2$ diluted in water. An ECAT EXACT HR (CTI Inc. Knoxville, USA) was used as the PET scanner, and the emission scan acquisition in the 2D mode was repeated every hour. Seven scans were performed. Before the first scan, approximately 207 MBq of $^{18}F_2$ with half-life of 109.8 min, water was injected. Each scan comprised 5 s × 50 frames and the total acquired time was 250 s so that the calculated image count at each location must be almost constant across frames ($\sim$0.05% change between adjacent frames and $\sim$3% between the first and last frames). 72 h after the first scan (when the radioactivity of ^{18}F became negligible), two 10-min transmission scans were performed.

Two AC maps were created to correct the attenuation using the data from the two 10-min transmission scans. Using these AC maps, two dynamic images were reconstructed by employing the FBP method from the same sinogram data. Corrections for randoms, dead time, scatters, and radioactivity decay to the start time of the first scan were applied, and the Gaussian filter with a filter width of 7 mm was used. For the obtained images, we defined the *j*th pixel value as $x_{i,j}^{n,k}$ with the *k*th frame ($k = 1, 2,\ldots,50$) at *n*th scan

($n = 1, 2, \ldots, 7$) with ith AC map ($i = 1, 2$). Each image had a matrix size of 128 × 128 × 47 with a pixel size of 1.8 × 1.8 × 3.38 mm.

The pixel-wise SD images ($s^n_{i,j}$) were computed from all the 50 frames of the dynamic images as;

$$s^n_{i,j} = \mathrm{SD}_{k=1,\ldots,50}[x^{n,k}_{i,j}] \quad (1)$$

where, $\mathrm{SD}_{k\in K}[y_k]$ is defined as a standard deviation of y_k over K.

We calculated N-indices from two datasets to test equivalence of N-index to pixel-wise SD when amount of data change in terms of either scan duration or activity concentration as: (a) one frame data of duration 5 s and (b) 25 frames data of duration 125 s. For the dataset (a), a subtracted image ($I^{n,5s}_j$) was created by subtracting the 24th frame data with the first AC map from the 25th frame data with the second AC map as:

$$I^{n,5s}_j = x^{n,25}_{1,j} - x^{n,24}_{2,j}. \quad (2)$$

The reason that we selected the 24th and 25th frames for the subtraction was to minimize the influence of physical decay in the pixel value. For the dataset (b), even-numbered frames with the first AC map and odd-numbered frames with the second AC map were summed in order to obtain two independent (but must be identical in terms of the radioactivity count at each location) images. By subtracting the two images, the subtracted image was created as:

$$I^{n,125s}_j = \frac{1}{25}\sum_{k\in\mathrm{odd}} x^{n,k}_{1,j} - \frac{1}{25}\sum_{k\in\mathrm{even}} x^{n,k}_{2,j}. \quad (3)$$

The reason that we summed the frames alternately was to minimize the influence of physical decay in the pixel value. The subtracted image has a mean value that is approximately and uniformly zero.

A circular region of interest (ROI) (10.7 cm in diameter, 3620 pixels) was placed in the brain region on a slice at the level of thalamus. The mean SD value (M^n_{SD}) of $s^n_{i,j}$ and the N-index ($\mathrm{NI}^{n,t}$) of $I^{n,t}$ inside the ROI were calculated and compared.

Subjects and PET procedure

For the CBF and $CMRO_2$ measurements, we performed a series of PET scans on six human subjects with cerebrovascular disease ($n = 6$, age = 69 ± 3 years, body weight = 64 ± 4 kg). The DARG approach [4, 11] was employed to compute the CBF and $CMRO_2$ images. An ECAT EXACT 47 (CTI Inc. Knoxville, USA), equipped with three rotating ^{68}Ge–^{68}Ga rod sources was used as the PET scanner. The PET procedures were approved by the ethics committee of the National Cardiovascular Center.

Transmission scans with multiple frames (60 s × 9 frames and 30 s × 2 frames) were performed for 10 min. After the transmission scan, a 4-min static emission scan along with $C^{15}O$ administration was performed. Subsequently, a dynamic DARG $H_2^{15}O$–$^{15}O_2$ scan [4] was started with the sequential administration of gaseous $^{15}O_2$ (3000 MBq, 1-min inhalation) followed by $H_2^{15}O$ (1110 MBq, intra-venous injection into the right brachial vein) administration after 6 min. The DARG scan sequence comprised 10 s × 6 frames, 20 s × 6 frames, 30 s × 4 frames, 10 s × 4 frames, 5 s × 10 frames and 15 s × 2 frames. All data were acquired in the 2D mode with extended septa.

To obtain the arterial input function, a catheter was inserted into the brachial artery, and blood was withdrawn at a flow rate of 4 ml/min during each emission PET scan. The arterial blood time activity curve (TAC) was continuously monitored using a GSO input function monitor [12].

Data processing

From the multi-frame transmission data with 11 frames, two sets for 30, 60, 120, 180, 240 and 300 s were generated by adding the frames and avoiding duplications. In addition, the sum of the transmission data with a duration of 600 s was obtained. On the basis of the obtained transmission data and the blank scan data, 13 AC maps were generated defined as AC^t_i, where $i = 1, 2$ (index of the sets), and $t = 30, 60, 120, 180, 240, 300$ s (transmission data time duration) and AC^{600s}_1.

Along with detector normalization, the static images for the $C^{15}O$ scan and the dynamic image for the $^{15}O_2$–$H_2^{15}O$ emission scan sinograms were corrected for dead time and radioactive decay in each frame. Tomographic images were reconstructed using these corrected sinograms obtained by the FBP method with 7-mm Gaussian filtering. AC was applied to the $C^{15}O$ static image using the AC map obtained from the 600-s transmission data, (i.e., AC^{600s}_1), and to the $^{15}O_2$–$H_2^{15}O$ dynamic image using all the generated AC map data of AC^t_i. Thus, 13 dynamic images were obtained. The pixel value was defined as $x^k_{j,(i,t)}$ for jth pixel value with kth frame using AC^t_i. A scatter correction was also applied. The reconstructed dynamic images had a matrix size 128 × 128 × 47 with a pixel size of 1.8 × 1.8 × 3.38 mm.

The following three steps were employed to sum up a part of the reconstructed dynamic image for the $^{15}O_2$–$H_2^{15}O$ scan during each oxygen (180 s from the start of oxygen inhalation, indicated as: $k \in O_2$) and water (120 s from the increase in the brain tissue TAC, indicated as: $k \in H_2O$) phase. First, all the frames were summed as: $\sum^{k\in O_2,\mathrm{all}} x^k_{j,(1,t)}$ and $\sum^{k\in H_2O,\mathrm{all}} x^k_{j,(1,t)}$. Second, all the even-numbered frames

were summed as: $\sum^{k\in O_2,\text{even}} x^k_{j,(2,t)}$ and $\sum^{k\in H_2O,\text{even}} x^k_{j,(2,t)}$. Lastly, all the odd-numbered frames were summed as: $\sum^{k\in O_2,\text{odd}} x^k_{j,(1,t)}$ and $\sum^{k\in H_2O,\text{odd}} x^k_{j,(1,t)}$. We assumed two images summed with even- and odd-numbered frames are physiologically and quantitatively equivalent and statistically independent.

Arterial blood TACs were corrected for radioactivity decay and dispersion ($\tau = 4$ s) [4, 13, 14] and delay [3, 4, 15] further, the $^{15}O_2$ and $H_2^{15}O$ contents were separated [11]. The obtained $^{15}O_2$ and $H_2^{15}O$ arterial TACs were used as the water and oxygen input functions as $A_W(t)$ and $A_O(t)$, respectively.

Sets of CBF, OEF and $CMRO_2$ images were generated using the DARG approach as described previously [4] by using a set of summed images in both the oxygen and water phases ($\sum^{k\in O_2,\rho} x^k_{j,(1,t)}$ and $\sum^{k\in H_2O,\rho} x^k_{j,(1,t)}$, where ρ indicates the rule of sum, i.e., all, even or odd), $^{15}O_2$ and $H_2^{15}O$ input functions [$A_W(t)$ and $A_O(t)$] and cerebral blood volume (CBV) image that was obtained from the $C^{15}O$ scan data [3, 4]. This procedure was repeated for all sets of images and the functional images for jth pixel were obtained as: $CBF^{\rho}_{j,(i,t)}$, $OEF^{\rho}_{j,(i,t)}$ and $CMRO^{\rho}_{2j,(i,t)}$, where indices (i, t) are same as those for AC, and ρ is the rule of sum.

Dependency of quantitative CBF/OEF/$CMRO_2$ accuracy on the transmission true counts

An ROI was placed on the frontal, temporal and parietal cortical region (5000–10000 pixels) of the image and the CBF, OEF and $CMRO_2$ values were extracted from all the datasets. The mean of these extracted values was expressed as the percent difference between the values obtained from the functional images computed with $AC^t_1$and with AC^{600s}_1 for all datasets obtained from the emission data as:

$$\frac{R\left[\text{Func}^{\text{all}}j_{j,(1,t)}\right] - R\left[\text{Func}^{\text{all}}_{j,(1,600s)}\right]}{R\left[\text{Func}^{\text{all}}_{j,(1,600s)}\right]} \times 100\% \quad (4)$$

where R indicates mean pixel value inside the ROI and Func indicates either CBF, OEF or $CMRO_2$.

Dependency of CBF/OEF/$CMRO_2$ image quality on the transmission true counts

Subtracted images were created by subtracting the functional images between even- and odd-numbered frames as;

$$I^{\text{Func}}_{j,t} = \text{Func}^{\text{even}}_{j,(1,t)} - \text{Func}^{\text{odd}}_{j,(2,t)} \quad (5)$$

for the jth pixel. The N-index in the ROI, placed on the frontal, temporal and parietal cortical region as above, for these subtracted images were calculated as:

$$\text{NI}^t_{\text{Func}} = \text{SD}_{j\in\text{ROI}}\left[I^{\text{Func}}_{j,t}\right]. \quad (6)$$

The obtained N-indices were expressed as a function of the total true count of the transmission scan data.

Results

Phantom studies for validation of N-index

Figure 1 shows representative slices of the obtained images of mean, SD, and subtraction. The later scan has more noise due to count statistics, which can be observed in SD image and the subtracted images in Fig. 1. Despite the difference in the activity distribution, the SD image was almost uniform. The relationship between the mean value of the SD image (M_{SD}) and N-index (NI) in the same ROI

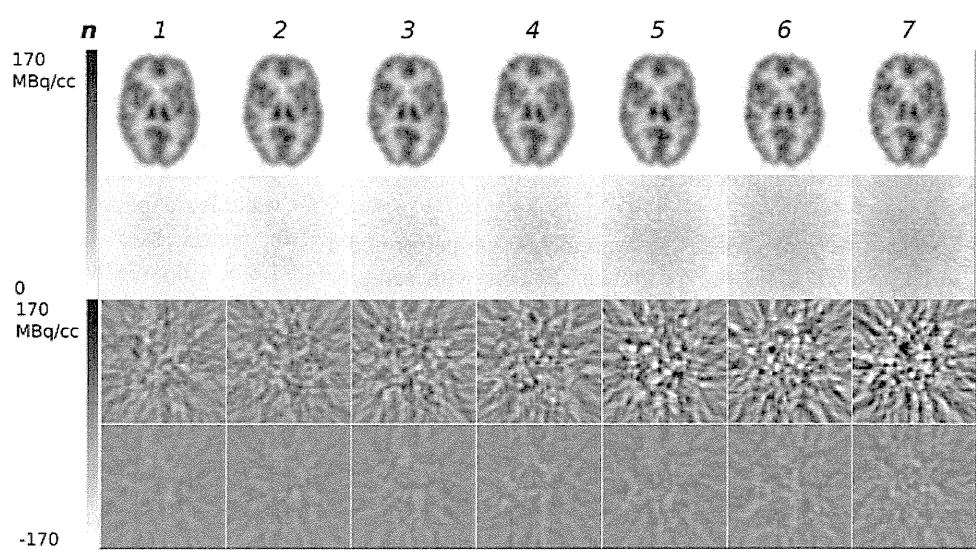

Fig. 1 Representative slices of the reconstructed images obtained from the phantom studies. The *first row* is averaged image, the *second row* is SD image, the *third row* is the subtracted image for the dataset (a), and the *fourth row* is the subtracted image for the dataset (b). *Each column* corresponds the images from nth scan (total seven scans)

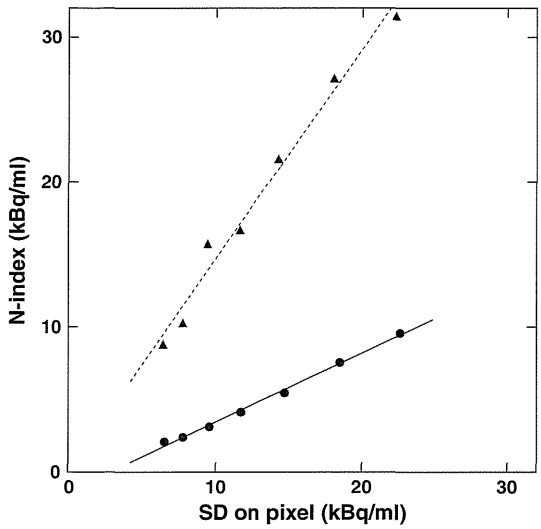

Fig. 2 The relationship between the mean SD value and *N*-index obtained from the subtracted image with the same ROI region of the brain phantom. The regression line was expressed as $y = 1.44x - 0.331$ (kBq/ml) ($r = 0.99$, $n = 7$). and $y = 0.47x - 1.29$ (kBq/ml) ($r = 0.99$, $n = 7$), for 5 s (*closed triangle*) and 125 s (*closed circle*) in calculating *N*-index, respectively

is shown in Fig. 2. The regression line is expressed as $NI = 1.44M_{SD} - 0.331$ (kBq/ml) ($r = 0.99$) and $NI = 0.47M_{SD} - 1.285$ (kBq/ml) ($r = 0.99$), where r is correlation coefficient, for the subtracted images obtained from the 5- and 125-s data, respectively. The results shown in Figs. 1 and 2 support the assumption that the SD of the pixel value is uniform in a non-homogeneous image that was reconstructed using the FBP method. Furthermore, the present *N*-index was correlated with the SD and could be employed to compare the image qualities.

Dependency of quantitative CBF/OEF/$CMRO_2$ accuracy on the transmission true counts

Figure 3 shows the percent difference in the CBF (a), OEF (b) and $CMRO_2$ (c) values when compared with those computed using the 10-min AC map. The results show that the quantitative values obtained during the CBF, OEF and $CMRO_2$ measurements are almost identical, namely, difference was <5% to those obtained when AC was performed using the transmission data containing true counts more than 40 Mcounts.

Dependency of the CBF/OEF/$CMRO_2$ image quality on the transmission true counts

Figure 4 shows the *N*-indices in the CBF (a), OEF (b) and $CMRO_2$ (c) images, as a function of the number of true counts of the transmission data. The present results show that the qualities of the CBF, OEF and $CMRO_2$ images

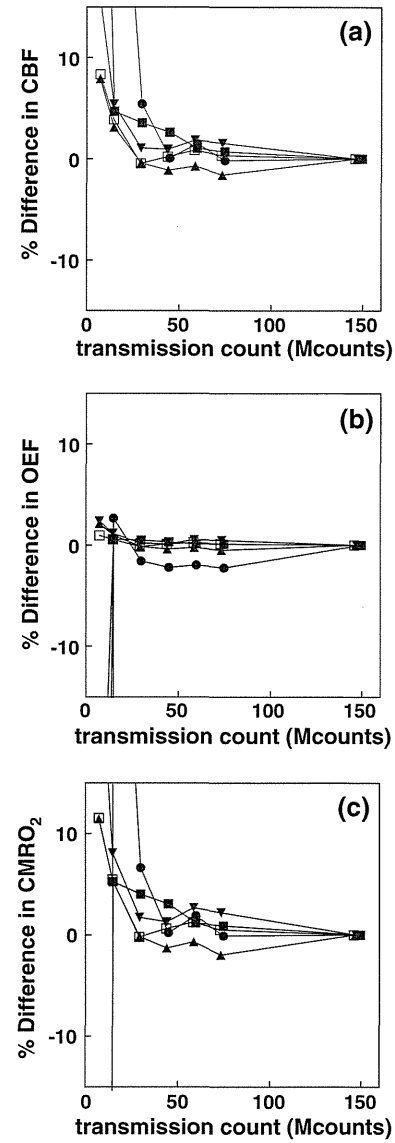

Fig. 3 Percent difference in the CBF, OEF and $CMRO_2$ values when compared with those obtained from the 10-min transmission data, as a function of the true counts of the transmission data. Each type of *symbol* corresponds to each subject ($n = 6$). The indicated values were extracted from the ROI in the frontal, parietal and temporal cortex regions

were almost equal to those in which the true counts of the transmission data used exceeded 40 Mcounts.

Discussion and conclusion

Our purpose of this study was to shorten the transmission scan duration for ^{15}OPET study with DARG measurement. By evaluating bias and noise on the functional images of the CBF, OEF and $CMRO_2$ due to noise in transmission data, optimal transmission true count in DARG measurement was

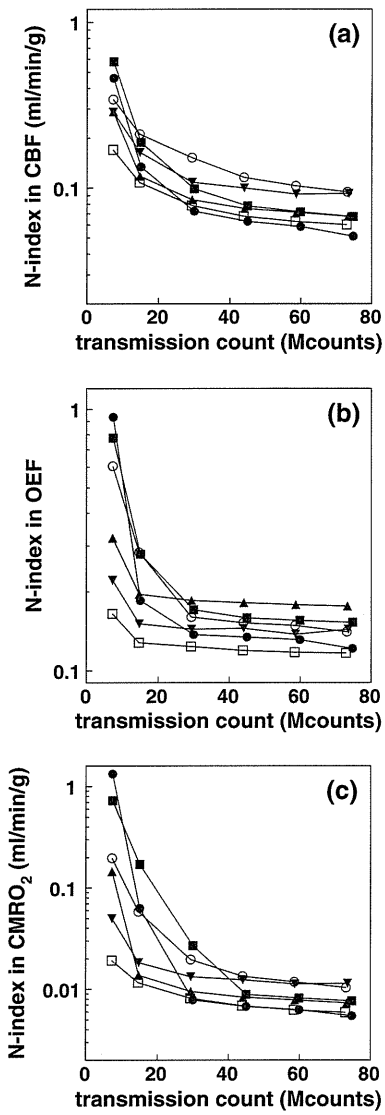

Fig. 4 The *N*-indices for the CBF, OEF and $CMRO_2$ images that were obtained from various true counts of the transmission data as a function of the true counts of the transmission data. Each type of *symbol* corresponds to each subject ($n = 6$). The *symbols* used and ROI are the same as that used for Fig. 3

determined. We found 40 Mcounts of the true count in the transmission scan was optimal, and consequently, we were able to shorten the total duration of the DARG examination.

We introduced the *N*-index to compare the noise level on inhomogeneous functional images. The benefit of using *N*-index is that by one index number, one can characterize the noise in functional image derived from PET data and DARG measurement which have complex noise propagations from several error sources. The validity of the *N*-index was tested in the phantom study. We found tight correlation between pixel noise and the *N*-index.

The present result using the brain phantom supported the assumption that the SD of a pixel value was spatially uniform even in a non-homogeneous region of an FBP reconstructed image (Fig. 1). Furthermore, the regression line between the SD value from the statistically obtained SD image and the *N*-index from the subtracted image for 5- and 125-s data were highly correlated ($r = 0.99$) (Fig. 2). The slope for 5-s data was approximately $\sqrt{2}$, where the SD of the image obtained by subtraction of two 5-s data (statistically corresponding to 10 s) could be expected to be $\sqrt{2}$ greater than that of the original image. For 125-s data, 1/5 of statistical noise compared to 5-s data is expected. However, *N*-index for 125-s data overestimated in 18% in average than expected. One possible reason of this overestimation is influence of inhomogeneity of the reconstructed image. Therefore, the *N*-index cannot be used to estimate absolute noise level in the image, but the *N*-index is still valid for study which compares relative noise levels among multiple images.

Using the *N*-index, we examined the change of image quality in the CBF, OEF and $CMRO_2$ as the noise level based on the change in the true counts of the transmission data. One of the advantages using the *N*-index is that it allows us to compare the noise level of non-uniform images such as that of the brain, using the data obtained by ordinal PET scan procedure. In order to investigate the noise level of the PET images using parameters other than the *N*-index, the PET scans must be replicated for a human subject. However, this appears unlikely due to the excessive radiation dose that would need to be administered to the subject. Furthermore, it might be quite hard to maintain the equivalent measurement conditions such as the radiation dose, as well as the physiological conditions of the subjects.

In this study, two implicit conditions were assumed: the SD on pixel value is uniform for the targeted region and odd-and even-numbered frames have the same statistical properties. The condition of uniform distribution of the SD on the functional image might not be microscopically fulfilled due to nature of nonlinearity of DARG method. However, in global, noise on the reconstructed image could be linearly propagated to the functional image and we considered this assumption was valid for computing the *N*-index. The *N*-index can be applied to other cases such as a variety of tracers and organs in order to examine the image quality as far as those conditions are satisfied. It should be noted that the CBF and $CMRO_2$ parametric images are required to be assessed quantitatively [16], thus the present study was validated with images reconstructed by FBP method. Limitation of the present method is that the *N*-index may not be applied to images such as those reconstructed by the maximum likelihood expectation maximization based algorithm, because the uniformity of SD across pixels is not guaranteed. However, a similar procedure of the present method still has possibility to be

applied, if, for example, coefficient of variation is uniform across pixels.

When *N*-index was estimated from two images with either emission or transmission data being common, the variation on image can be calculated as a sum of each variation and subtraction of covariance, canceling effect of noise from common data. Consequently, the *N*-index only reflects noise on either transmission or emission data. Thus, we estimated *N*-index by subtracting fully independent images. The validity of *N*-index could be tested in the phantom study using common transmission data; however, we still computed *N*-index using fully independent images, because the test should be done in the same conditions as the experimental study.

The present results showed that poor count statistics in transmission scanning resulted in significant bias in quantitative values of CBF, OEF and $CMRO_2$. As has been mathematically described [17], AC factor, i.e. blank/transmission is biased by factor of $(1 + 1/m)$, where m is a transmission count on a corresponding pixel. Therefore, the poorer the transmission scan count is, the higher the AC factor becomes. In view of image quality, noise in transmission data influences functional image as shown in Fig. 4. On the other hand, as indicated in Fig. 4, extra longer transmission scan gains no statistical benefit. The optimized transmission scan duration will be determined by relative noise level of the transmission data against the emission data.

In this paper, we used fixed duration of 600 s of the transmission scan for CO image, assuming little effect of noise on CO image. One reason for this assumption is that 50% error in CBV value derives around only 3% error in OEF and $CMRO_2$ images [4], suggesting 50% noise on CBV image resulting only 3% noise on OEF and $CMRO_2$ images. As shown in Fig. 4, the degree of noise on the OEF and $CMRO_2$ images are around 20–25%, and the level of noise is quite high compared to level of noise from CBV image.

Motion of subject, during a scan, could be a problem to calculate *N*-index. However, movement of a subject during a scan affects both the odd-and even-numbered frames simultaneously, and thus the statistical properties between two summed images will stay the same. Thus, motion of a subject during a scan might not be that critical with regards to the *N*-index, as far as the motion does not deteriorate the image used to assess the function of the targeted organ.

The comparison of the *N*-indices between subjects or between different functional images cannot be performed because the *N*-indices offer information of relative noise level but not absolute noise. Thus, a meaningful comparison can be made between images of the same subject and of the same cerebral function (such as CBF and $CMRO_2$).

It is generally accepted that accurate ACs require transmission scanning using external sources [6, 7], although there are excellent techniques designed to shorten or eliminate the transmission scan duration, such as the transmission-data-based segmented method for the AC map [18, 19] or the emission-based AC map calculation [20]. The present approach might be applicable to investigate the noise level in segmented or emission-based methods, which should enable us to further shorten the duration of a PET examination.

Boellaard et al. demonstrated the relationship between the transmission scan counts and phantom diameter, and they found that this relationship did not restrict the application of the count-based transmission scans for correcting the reduction in the rod source strength [21]. However, they indicated that when the subject is extremely small, a transmission scan based on an acquired number of true counts should not be applied. This is because the counts for lines of response not passing through the subject would increase. Further studies are required to determine the optimal examination conditions for such situations.

We found that the true counts of the transmission data exceeding 40 millions (corresponds to 3 min scan in this study) were appropriate for the CBF, OEF and $CMRO_2$ measurement by DARG method in terms of both quantitative accuracy and image quality, consequently we can shorten the examination duration for obtaining those images. Conventional DARG measurement in clinical study uses 10 min of transmission scan, while 9 min of emission scan of dual tracers of $^{15}O_2$ and $H_2^{15}O$, in addition to 4 min of $C^{15}O$ scan [22]. If one can shorten the transmission scan to 3 min, total scan duration is 16 min (30% reduction). Currently, another $C^{15}O$ scan for CBV correction with regards to the assessment of CBF, OEF and $CMRO_2$ is still required, an additional mathematical formulation strategy, like the basis function method [23] could eliminate this requirement [5].

In conclusion, we determined the required transmission true count that maintains the quantitative accuracy and image quality for PET studies with $H_2^{15}O$ and $^{15}O_2$. According to our results, the total study duration could be minimized by shortening the transmission scan. Although the obtained results in the present study were measurement condition specific, the *N*-index could be used to determine PET scanning procedures.

Acknowledgments The authors would like to thank Ms Atra Ardakani for her invaluable help on preparing this article. The authors gratefully acknowledge the staff of the Department of Nuclear Medicine, Hospital and the Department of Investigative Radiology, Research Institute, National Cardiovascular Center. The present work was supported by the Program for Promotion of Fundamental Studies in Health Science of the Organization for Pharmaceuticals and

Medical Devices Agency of Japan (PMDA), and the Nakatani Electronic Measuring Technology Association of Japan, and by the Ministry of Education, Science, Sports and Culture, Grant-in-Aid for Young Scientists (start-up), 21890171, 2009.

References

1. Mintun M, Raichle M, Martin W, Herscovitch P. Brain oxygen utilization measured with O-15 radiotracers and positron emission tomography. J Nucl Med. 1984;25:177–87.
2. Hatazawa J, Fujita H, Kanno I, Satoh T, Iida H, Miura S, et al. Regional cerebral blood flow, blood volume, oxygen extraction fraction, and oxygen utilization rate in normal volunteers measured by the autoradiographic technique and the single breath inhalation method. Ann Nucl Med. 1995;9:15–21.
3. Shidahara M, Watabe H, Kim K, Oka H, Sago M, Hayashi T, et al. Evaluation of a commercial PET tomograph-based system for the quantitative assessment of rCBF, rOEF and rCMRO2 by using sequential administration of 15O-labeled compounds. Ann Nucl Med. 2002;16:317–27.
4. Kudomi N, Hayashi T, Teramoto N, Watabe H, Kawachi N, Ohta Y, et al. Rapid quantitative measurement of CMRO(2) and CBF by dual administration of (15)O-labeled oxygen and water during a single PET scan—a validation study and error analysis in anesthetized monkeys. J Cereb Blood Flow Metab. 2005;25:1209–24.
5. Kudomi N, Hayashi T, Watabe H, Iida H. Rapid CBF/$CMRO_2$ measurement in a single PET scan with dual tracer administration. J Cereb Blood Flow Metab. 2005;25:S672.
6. Bailey D. Transmission scanning in emission tomography. Eur J Nucl Med. 1998;25:774–87.
7. Ostertag H, Kbler W, Doll J, Lorenz W. Measured attenuation correction methods. Eur J Nucl Med. 1989;15:722–6.
8. Watabe H, Matsumoto K, Senda M, Iida HP. Performance of list mode data acquisition with ECAT EXACT HR and ECAT EXACT HR + positron emission scanners. Ann Nucl Med. 2006;20:189–94.
9. Hoffman E, Cutler P, Digby W, Mazziotta J. 3-D phantom to simulate cerebral blood flow and metabolic images for PET. IEEE Trans Nucl Sci. 1990;37:616–20.
10. Pajevic S, Daube-Witherspoon M, Bacharach S, Carson R. Noise characteristics of 3-D and 2-D PET images. IEEE Trans Med Imaging. 1998;17:9–23.
11. Kudomi N, Watabe H, Hayashi T, Iida H. Separation of input function for rapid measurement of quantitative $CMRO_2$ and CBF in a single PET scan with a dual tracer administration method. Phys Med Biol. 2007;52:1893–908.
12. Kudomi N, Choi E, Yamamoto S, Watabe H, Kim K, Shidahara M, et al. Development of a GSO detector assembly for a continuous blood sampling system. IEEE Trans Nucl Sci. 2003;50:70–3.
13. Iida H, Kanno I, Miura S, Murakami M, Takahashi K, Uemura K. Error analysis of a quantitative cerebral blood flow measurement using H2(15)O autoradiography and positron emission tomography, with respect to the dispersion of the input function. J Cereb Blood Flow Metab. 1986;6:536–45.
14. Lammertsma A, Cunningham V, Deiber M, Heather J, Bloomfield P, Nutt J, et al. Combination of dynamic and integral methods for generating reproducible functional CBF images. J Cereb Blood Flow Metab. 1990;10:675–86.
15. Iida H, Higano S, Tomura N, Shishido F, Kanno I, Miura S, et al. Evaluation of regional differences of tracer appearance time in cerebral tissues using [15O] water and dynamic positron emission tomography. J Cereb Blood Flow Metab. 1988;8:285–8.
16. Ibaraki M, Miura S, Shimosegawa E, Sugawara S, Mizuta T, Ishikawa A, et al. Quantification of cerebral blood flow and oxygen metabolism with 3-dimensional PET and 15O: validation by comparison with 2-dimensional PET. J Nucl Med. 2007;49:50–9.
17. Freedman N, Bacharach S, Carson R, Price J, Dilsizian V. Effect of smoothing during transmission processing on quantitative cardiac PET scans. J Nucl Med. 1996;37:690–4.
18. Xu M, Luk W, Cutler P, Digby W. Local threshold for segmented attenuation correction of PET imaging of the thorax. IEEE Trans Nucl Sci. 1994;41:1532–7.
19. Xu M, Cutler P, Luk W. Adaptive, segmented attenuation correction for whole-body PET imaging. IEEE Trans Nucl Sci. 1996;43:331–6.
20. Weinzapfel B, Hutchins G. Automated PET attenuation correction model for functional brain imaging. J Nucl Med. 2001;42:483–91.
21. Boellaard R, Lingen Av, Balen Sv, Lammertsma A. Optimization of attenuation correction for positron emission tomography studies of thorax and pelvis using count-based transmission scans. Phys Med Biol. 2004;49:N31–8.
22. Iwanishi K, Watabe H, Hayashi T, Miyake Y, Minato K, Iida H. Influence of residual oxygen-15-labeled carbon monoxide radioactivity on cerebral blood flow and oxygen extraction fraction in a dual-tracer autoradiographic method. Ann Nucl Med. 2009;23:363–71.
23. Gunn R, Lammertsma A, Hume S, Cunningham V. Parametric imaging of ligand receptor binding in PET using a simplified reference region model. Neuroimage. 1997;6:279–87.

Multicenter Evaluation of a Standardized Protocol for Rest and Acetazolamide Cerebral Blood Flow Assessment Using a Quantitative SPECT Reconstruction Program and Split-Dose ^{123}I-Iodoamphetamine

Hidehiro Iida[1,2], Jyoji Nakagawara[1,3], Kohei Hayashida[1,4], Kazuhito Fukushima[1,5], Hiroshi Watabe[1,2], Kazuhiro Koshino[1,2], Tsutomu Zeniya[1,2], and Stefan Eberl[1,6]

[1]Dual-Table Autoradiography SPECT Research Group in Japan, Osaka, Japan; [2]National Cerebral and Cardiovascular Center–Research Institute, Osaka, Japan; [3]Nakamura Memorial Hospital, Sapporo, Japan; [4]Takeda Hospital, Kyoto, Japan; [5]National Cerebral and Cardiovascular Center–Hospital, Osaka, Japan; and [6]Royal Prince Alfred Hospital, Sydney, Australia

SPECT can provide valuable diagnostic and treatment response information in large-scale multicenter clinical trials. However, SPECT has been limited in providing consistent quantitative functional parametric values across the centers, largely because of a lack of standardized procedures to correct for attenuation and scatter. Recently, a novel software package has been developed to reconstruct quantitative SPECT images and assess cerebral blood flow (CBF) at rest and after acetazolamide challenge from a single SPECT session. This study was aimed at validating this technique at different institutions with a variety of SPECT devices and imaging protocols. **Methods:** Twelve participating institutions obtained a series of SPECT scans on physical phantoms and clinical patients. The phantom experiments included the assessment of septal penetration for each collimator used and of the accuracy of the reconstructed images. Clinical studies were divided into 3 protocols, including intrainstitutional reproducibility, a comparison with PET, and rest–rest study consistency. The results from 46 successful studies were analyzed. **Results:** Activity concentration estimation (Bq/mL) in the reconstructed SPECT images of a uniform cylindric phantom showed an interinstitution variation of ±5.1%, with a systematic underestimation of concentration by 12.5%. CBF values were reproducible both at rest and after acetazolamide on the basis of repeated studies in the same patient (mean ± SD difference, −0.4 ± 5.2 mL/min/100 g, n = 44). CBF values were also consistent with those determined using PET (−6.1 ± 5.1 mL/min/100 g, n = 6). **Conclusion:** This study demonstrates that SPECT can quantitatively provide physiologic functional images of rest and acetazolamide challenge CBF, using a quantitative reconstruction software package.

Key Words: ^{123}I-iodoamphetamine; cerebral blood flow; acetazolamide; SPECT; vascular reactivity; quantitation

J Nucl Med 2010; 51:1624–1631
DOI: 10.2967/jnumed.110.078352

Received Apr. 27, 2010; revision accepted Jul. 14, 2010.
For correspondence or reprints contact: Hidehiro Iida, Department of Investigative Radiology, National Cerebral and Cardiovascular Center–Research Institute, 5-7-1 Suita City, Osaka 565-8565, Japan.
E-mail: iida@ri.ncvc.go.jp

Current clinical practice using SPECT relies largely on interpretation of qualitative images reflecting physiologic function. Quantitative functional parametric images may be obtained by applying mathematic modeling to SPECT data corrected for attenuation and scatter. Quantitative regional cerebral blood flow (CBF) (*1–3*) and cerebral vascular reactivity (CVR) in response to acetazolamide challenge (*4–6*) have been obtained with these techniques. One major application of such quantitative SPECT (QSPECT) approaches is the evaluation of ischemic status in patients with occlusion or stenosis in their middle cerebral arteries, to provide prognostic information of the outcome of revascularization therapies (*7*). Quantitative analysis in SPECT has also been demonstrated in the assessment of binding potential for several neuroreceptor ligands (*8,9*), for the quantitative assessment of regional myocardial perfusion (*10,11*), and for the assessment of radioaerosol deposition and clearance in healthy and diseased lungs (*12*). However, providing the standardized quantitative approach required for multicenter clinical trials has so far received only limited attention. Challenges remain in providing consistent quantitative data across institutions using a variety of SPECT equipment and vendor-specific reconstruction strategies (*13*). This limitation is attributed to a lack of standardized procedures in the reconstruction software offered by vendors, particularly in terms of correcting attenuation and scatter. Kinetic modeling for physiologic parameter estimation is also not part of the vendors' standard SPECT software. Although separate packages can be purchased for this purpose, they are not integrated and are flexible general-purpose packages, requiring considerable skill and knowledge to effectively use. Thus, they are not ideal for routine clinical use.

Scatter and attenuation occur in the object and are thus object-dependent but are not dependent on the geometry of the imaging equipment (*14*). Therefore, once a software program is developed to provide accurate image reconstruction with compensation for both attenuation and scatter, the

program should be able to provide quantitative images that are intrinsically independent of the geometric design of SPECT cameras. This is an attractive feature of SPECT for multicenter clinical studies.

From the various techniques available to correct for attenuation (*15*) and scatter (*16*), one feasible approach for clinical studies is based on a combination of attenuation correction, incorporated into the ordered-subset expectation maximization (OSEM) reconstruction (*17*), and scatter correction by the transmission-dependent convolution subtraction (TDCS) originally proposed by Meikle et al. (*18*). This approach has been extensively investigated by our group (*11,19*) for ^{99m}Tc for studies of the brain and heart (*18,20*) and also in cardiac ^{201}Tl studies (*11,21*). A recent study also demonstrated the accuracy of this approach in a combined SPECT/CT system (*22*). By incorporating a correction for collimator septal penetration by high-energy emissions, one can also make the technique applicable to ^{123}I (*19*).

The QSPECT reconstruction approach has estimated CBF images at rest in a clinical setting (*11*) and quantified CVR by measuring CBF at rest and after vasodilation in a single SPECT session. This was accomplished by using the dual-table autoradiographic (DTARG) method and a dual administration of ^{123}I-iodoamphetamine (*23*). In those studies, corrections for attenuation and scatter appeared to be essential for generating quantitative CBF maps that were consistent with those generated by ^{15}O-water PET (*11,23*).

These studies were, however, validated in a single institution using a limited range of SPECT systems, and the general applicability of this technique for different SPECT systems had yet to be fully established. Thus, the aim of this study was to verify that analysis of data with a standardized reconstruction package incorporating attenuation and scatter correction can provide reproducible results across multiple institutions for quantitative rest and acetazolamide challenge CBF estimation from a single SPECT session.

MATERIALS AND METHODS

Institutions and Subjects

The 12 participating institutions were clinical centers and generally did not have scientific staff dedicated to nuclear medicine software or hardware development. Standard, vendor-supplied software was used for the collection of the studies, with unmodified scanners and collimators clinically used for brain studies. The acquired data were reconstructed with the program package developed for this project. Manufacturers and models of camera systems and the number of detectors and collimators (including fanbeam or parallel hole) used by the institution are listed in Supplemental Table 1 (supplemental materials are available online only at http://jnm.snmjournals.org). All institutions performed experiments on physical phantoms according to the protocol described in the "Phantom Experiment" section. Of the 12 institutions, 9 obtained patient scans, whereas the remaining 3 provided only phantom data. Clinical studies were approved by institutions' ethics committees or followed guidelines for clinical research protocols authorized by the institution. All subjects at each institution gave written informed consent.

The clinical studies were divided into 3 protocols: intrainstitutional, intrasubject reproducibility (reproducibility); comparison with PET (vs. PET); and intrascan consistency of the dual-time-point split-dose (rest–rest). Studies were excluded from the analysis if there was severe patient motion during one of the studies or if there were changes in the condition of the patients between the first and second studies likely to lead to changes in CBF.

Eight institutions (institutions 1, 3, 4, 6, 8, 9, 11, and 12) participated in the reproducibility arm, in which quantitative CBF values measured on separate days were compared. In this arm, all patients experienced unilateral or bilateral stenosis or occlusion in the extracranial internal carotid artery. The patients' ages ranged from 43 to 81 y (mean ± SD, 65 ± 9 y). A total of 31 studies in this protocol were analyzed. Four patients had to be excluded from the analysis—2 because of significant changes in their pathophysiologic status between the studies and 2 because of severe motion and mispositioning in the scanner.

One institution (institution 4) performed the versus-PET studies. CBF values obtained by the DTARG method were compared with those by ^{15}O-water and PET. Studies were performed on 6 patients (5 men, 1 woman; age range, 71–74 y; mean age ± SD, 72 ± 1 y) with stenosis or occlusion of the extracranial internal carotid artery unilaterally (n = 3) or bilaterally (n = 3).

Two institutions (institutions 2 and 12) provided data for the rest–rest comparison. Five patients from institution 2 had chronic cerebral infarction, whereas 4 subjects from institution 12 had no sign of cerebral disease. Patients' ages ranged from 32 to 72 y (mean ± SD, 52 ± 15 y); 5 patients were men and 4 women.

Phantom Experiment

Three experiments were performed by each institution using the SPECT camera fitted with the collimators normally used in clinical brain studies. The first scan determined the absolute sensitivity or the becquerel calibration factor (BCF) of the reconstructed images. For 10 min, a 360° projection set was acquired of a syringe filled with a ^{123}I-iodoamphetamine solution of known radioactivity and placed at the center of the field of view. The syringe was supplied by Nihon-Medi Physics, and its radioactivity was calibrated to 111 MBq at noon on the day before the experiment, with an accuracy better than 3%, decaying to approximately 30 MBq at the time of the experiment, avoiding the dead time of the camera. The BCF was determined by dividing the absolute radioactivity by the total counts for the syringe region in the reconstructed image.

The second experiment determined the collimator septal penetration contribution (*24*) from high-energy photons into the primary 159-keV energy window for ^{123}I. A line-spread function was obtained from the projection data of a line source filled with ^{123}I-iodoamphetamine. The septal penetration was determined from the background level as described previously (*19*). A projection line-spread function was also generated from this line source placed in a water-filled cylindric phantom (diameter, 16 cm).

The third experiment used a 16-cm-diameter, 15-cm-long uniform cylindric phantom. The whole radioactivity used for the BCF determination was diluted into the phantom, and projection data were acquired for 30 min, using the clinical scan protocols described in the "Clinical Studies" section. The radioactivity concentration (counting rate per unit mass) of an approximately 0.3-mL sample from the phantom was measured using the well counters available at the various institutions. Both NaI- and plastic scintillator–based well counters were used (Supplemental Table

1). Average pixel counts derived from regions of interest on the reconstructed emission images were referred to the well counter radioactivity counting rate, to determine the cross-calibration factor between the SPECT images and well counter system. This cross-calibration factor was subsequently used for the blood sample counts of the clinical studies. Uniformity of the reconstructed emission images was evaluated.

Clinical Studies

All clinical SPECT studies followed the DTARG protocol, with dual administration of iodoamphetamine (*23*), depicted in Figure 1. Briefly, 2 dynamic scans were acquired in quick succession, with a 2-min interval between the scans. The first scan covered the initial 0- to 28-min period, and the second was acquired from 30 to 58 min. At 4 min per frame, 7 frames covered each of the 2 dynamic scan periods. ^{123}I-iodoamphetamine (111 MBq at institutions 2–12 or 167 MBq at institution 1) was infused twice over 1 min into the antecubital vein at 0 and 30 min. Acetazolamide (17 mg/kg, 1,000 mg maximum) was administered intravenously at 20 min after the first iodoamphetamine injection, corresponding to 10 min before the second iodoamphetamine injection. Projection data were summed for the acquisition duration of the first and second scans and reconstructed as described in the "QSPECT Reconstruction" section. In contrast to the study of Kim et al. (*23*), which used full arterial blood sampling, the individual arterial input functions were derived from a population-based standardized input function scaled with the whole-blood counts from a single arterial blood sample taken at approximately 10 min (*1,25–28*). This sample was also used for arterial blood gas analysis.

In the reproducibility arm, an additional, non-DTARG CBF study was performed on a separate day. Instead of DTARG, the previously reported ^{123}I-IMP autoradiographic (IMPARG) method (*1,19,25*) was performed within a month of the DTARG study. The IMPARG method is essentially equivalent to the present DTARG method, except that the IMPARG method uses a single iodoamphetamine administration to assess CBF either at rest or after acetazolamide challenge. The same image reconstruction process as for the DTARG protocol was used. In 12 studies, the DTARG protocol was used instead of IMPARG—namely, the DTARG study was performed twice to assess the CBF reproducibility at rest and after acetazolamide.

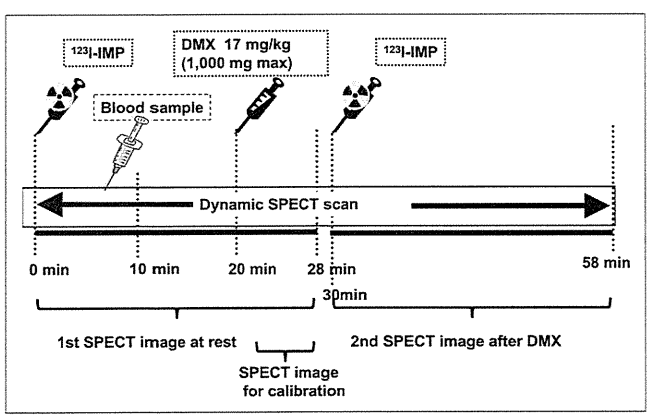

FIGURE 1. Scanning protocol flow for DTARG procedure. ^{123}I-iodoamphetamine was injected at 0 min, and 28-min resting dynamic SPECT scan was commenced. Blood sample for calibration of population input function was drawn at 10 min. Acetazolamide (DMX-diamox) was administered at 20 min. CBF values are scaled by last frame (time, 24–28 min). Second dynamic SPECT scan followed second injection of ^{123}I-iodoamphetamine at 30 min. IMP = iodoamphetamine.

In the versus-PET protocol, the PET study was performed within 2 d of the DTARG SPECT study. PET scans used intravenous ^{15}O-water both at rest and after the acetazolamide challenge. CBF images were calculated by the ^{15}O-water autoradiography technique (*29*), with careful corrections for delay and dispersion (*30–32*). Patients were stable between the SPECT and PET studies.

In the rest–rest protocol, the DTARG scan was obtained without the pharmacologic challenge during the study to evaluate the consistency of CBF values estimated from the 2 scans.

QSPECT Reconstruction

The program package for QSPECT uses a wrapper written in JAVA to run several programs written in C for Microsoft Windows systems. The package includes programs for reconstructing SPECT images, calculating functional images, coregistering images, and reslicing and printing summary logs.

The QSPECT package reconstructs images from the original projection data from commercial SPECT equipment, based on previous work by Iida and his colleagues (*19–21,23,33,34*). Reconstructed SPECT images are calibrated in Bq/mL, which provides independence from scanning parameters such as the acquisition time, number of views, matrix size, and zoom factor. Uniformity and center-of-rotation corrections and fanbeam–to–parallel beam conversion (for fanbeam collimators) were performed using the clinical routine software before reconstruction by this package.

An overall flow diagram of the correction and reconstruction process is shown in Supplemental Figure 1. The OSEM reconstruction technique includes attenuation correction (*17*). A threshold-based edge-detection algorithm generated the attenuation μ-map, assuming a uniform attenuation coefficient of 0.166 cm^{-1} for ^{99m}Tc (0.160 cm^{-1} for ^{123}I) as an average over the brain and skull (*19*). The threshold was optimized via the user interface to correctly define the brain outline. The attenuation μ-map was generated from the summed 0- to 28-min rest frame and was coregistered to the other images (*35*) reconstructed with filtered backprojection without attenuation or scatter correction. The attenuation μ-maps were forward projected to provide the transmission projection data for TDCS. The emission projections were scatter-corrected by the TDCS method, as originally proposed by Meikle et al. (*18*), and further optimized for realistic ^{99m}Tc, ^{201}Tl, and ^{123}I data in the brain and thorax regions (*20,21,23,33,34*). An offset compensated for the septal penetration of high-energy photons for ^{123}I studies, which adds fairly uniform background counts, or direct current (DC) components, to the projections.

Scatter- and attenuation-corrected images were reconstructed with OSEM (5 iterations, 5 subsets using geometric-mean projections, postreconstruction gaussian filter of 7 mm in full width at half maximum) and then realigned to the image set obtained from the first scan. The acquisition parameters and BCF were used to convert the reconstructed raw counts to Bq/mL.

The global CBF over the entire gray matter was estimated from the SPECT frame covering 24–28 min, because this timing minimizes the individual shape variations in individual input function. The look-up table generated for estimating CBF images from the complete dynamic study (0–28 min) was then

scaled to provide global cortical gray matter CBF values consistent with the 24- to 28-min frame estimates. A careful detection algorithm was used to reliably exclude extracranial accumulation of ^{123}I-iodoamphetamine (e.g., in the parotid region), which could adversely affect this scaling procedure. The regional CBF was then estimated at each pixel by means of the table look-up procedure (*25,28*). The background image at the time of the second ^{123}I-iodoamphetamine injection was estimated from the first-phase CBF images, according to the compartment model assumed in this study (*23*). An additional table look-up procedure was applied to the second dynamic dataset (30–58 min) for calculating the vasodilated (acetazolamide challenge) CBF images as described previously (*23*). The data were successfully reconstructed, and CBF was estimated at each institution. To facilitate and provide consistent analysis, the data presented are from the reanalysis conducted at the core lab (National Cerebral and Cardiovascular Center).

Data Analysis

The uniform phantom SPECT activity estimates were compared with the known activity in the phantom. Images for the baseline study were displayed with subsequent images using an absolute flow value scale to visually ascertain regional and global differences in flow. Regions of interest were placed on the middle cerebral artery territories of both hemispheres, and the average flow values between the different methods were compared and plotted. Bland–Altman plots and the SD of the differences evaluated the consistency of CBF values obtained from the reproducibility and versus-PET protocols.

All data were presented as mean ± SD. Pearson correlation analysis and linear regression analysis were used to evaluate relationships between the 2 CBF values. A P value less than 0.05 was considered statistically significant.

RESULTS

Phantom Studies

In the 16-cm scattering cylinder line source experiment, the scatter-uncorrected images show background counts extending beyond the phantom, from septal penetration of the high-energy photons. The scatter correction is largely effective in correcting for scatter and septal penetration counts. As shown in Supplemental Figure 2, the Toshiba-ECAM low- to medium-energy general-purpose (LMEGP) collimator, designed for reduced ^{123}I septal penetration, compared with the standard low-energy high-resolution collimator (GE Healthcare), demonstrates reduced scatter and septal penetration counts. The lower septal penetration of the Toshiba-ECAM LMEGP collimators is also supported by a lowered scatter correction offset value (DC = 0.05, compared with DC = 0.20 for the GE low-energy high-resolution collimator). The reduced scatter and septal penetration result in more complete removal of scatter for the LMEGP collimator.

Figure 2 displays reconstructed slices of the uniform phantom for all 12 institutions, scaled to the same maximum activity concentration. The estimated activity concentrations from these studies, compared with the known activity concentration, represented an accuracy of 87.5% ± 5.1% (Supplemental Table 1). The well counter–to–SPECT cross-calibration factor, which represents the sensitivity of the well counter system for ^{123}I, was 0.5–1.0 for NaI systems and 0.1–0.2 for plastic scintillation detector systems. The BCF values were consistent for the same SPECT camera–collimator configurations.

Clinical Studies

Figure 3A shows typical CBF images obtained at 4 institutions with 4 different γ-camera vendors, performed as part of the reproducibility arm of the study. Each case shows different CBF distributions both at rest and after acetazolamide challenge. The acetazolamide images obtained using the DTARG method agree well with the images subsequently obtained with the IMPARG method after acetazolamide infusion.

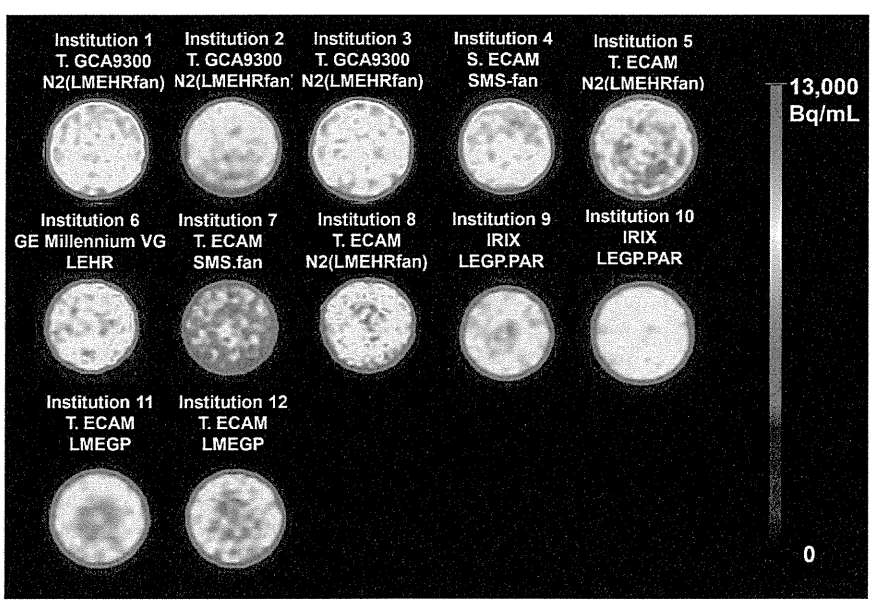

FIGURE 2. Reconstructed slices through uniform phantom from the participating 12 institutions. Experiment was designed to have same phantom activity concentration for each center's study. Nonuniformities and also differences in absolute activity concentration estimates can be observed, highlighting need for rigorous calibration, flood correction, and quality control. Legend above each image gives institution number (given in Supplemental Table 1), γ-camera model, and collimator used.

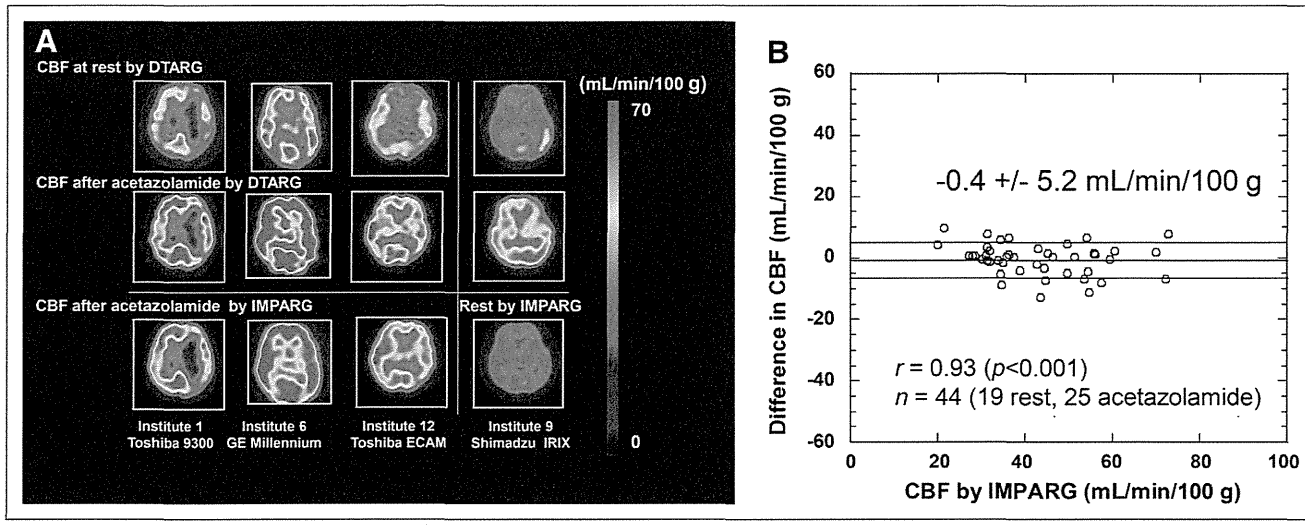

FIGURE 3. (A) Images from reproducibility study. CBF images obtained at rest and after acetazolamide with DTARG method. Repeated scan (third row) within 1 mo using IMPARG method and acetazolamide stress (columns 1–3) and at rest (last column). Images demonstrate that CVR can be estimated with this technique and demonstrate good reproducibility of measuring both at rest and after acetazolamide challenge CBF. (B) Bland–Altman plot showing difference vs. IMPARG CBF values estimated from DTARG method and repeated IMPARG studies to assess reproducibility. Little systematic bias is detected (mean difference, −0.4 mL/100 g/min), and SD of differences is moderate (5.2 mL/100 g/min). Correlation coefficient of $r = 0.93$ ($P < 0.001$) was found.

CBF images of a subject with left middle cerebral artery occlusion are shown in Supplemental Figure 3 for slices covering the whole brain. The images demonstrate reduced CBF after acetazolamide challenge in the left middle cerebral artery territory. The good reproducibility is confirmed by the Bland–Altman plot comparison of DTARG CBF values, with the CBF values obtained at a different imaging session with IMPARG or DTARG (Fig. 3B). The SD of the differences is 5.2 mL/100 g/min, with low bias supported by the mean difference of 0.4 mL/100 g/min. Regression analysis between DTARG and IMPARG values yielded a significant correlation ($P < 0.001$), with a correlation coefficient of $r = 0.93$.

Figure 4A shows MR and CBF images at rest and after acetazolamine obtained with DTARG SPECT and ^{15}O-water PET in a 73-y-old male patient (63 kg) with right internal carotid artery occlusion and left internal carotid stenosis. The MR images do not show any evidence of cerebral infarction in either hemisphere. Rest CBF was reduced bilaterally in the frontal-to-parietal regions, and acetazolamide increased CBF in left parietal regions but not in the right parietal area. DTARG CBF indicated the loss of vasoreactivity in the right internal carotid artery stenotic area. These findings were consistent with those from the PET evaluation. An additional example is shown in Supplemental Figure 4 for a 74-y-old female patient (48 kg) with left internal carotid artery stenosis, for whom MR images did not show cerebral infarction. DTARG CBF demonstrated preserved CBF in both hemispheres but reduced CBF reactivity in the left middle cerebral artery territory. The findings were again consistent with those from PET. Figure 4B compares the flow values obtained at rest and after acetazolamide with DTARG with the corresponding values obtained by ^{15}O-water PET. The SD of the differences is 5.1 mL/100 g/min, with the significant underestimation by ^{15}O-water PET, compared with PET by the DTARG method, highlighted by a mean difference of −6.1 mL/100 g/min. The Pearson analysis showed a significant correlation ($P < 0.001$), with a correlation coefficient of $r = 0.88$.

The results from the rest–rest protocol are summarized in Figure 5. The differences between the measurements performed with the 2 injections were small, with good agreement between the 2 flow values. The mean ± SD of the differences was 0.6 ± 2.9 mL/100 g/min.

DISCUSSION

The QSPECT package provided quantitative images consistent between the participating centers, using dual- or triple-detector SPECT scanners and collimators routinely used for nonquantitative brain studies. All centers successfully acquired the dynamic SPECT images, and the data from the variety of cameras encountered were successfully processed by the software package. Rest CBF and CVR could be readily obtained by the participating institutions in a single, clinically practical, 1-h scanning session. Good reproducibility of CBF estimates was observed in 31 pairs of studies at 8 institutions (Fig. 3), and the CBF estimated with the ^{123}I-iodoamphetamine SPECT agreed well with ^{15}O-water PET CBF at 1 institution (Fig. 4). The CBF values after the second injection of the DTARG were consistent with the values obtained after the

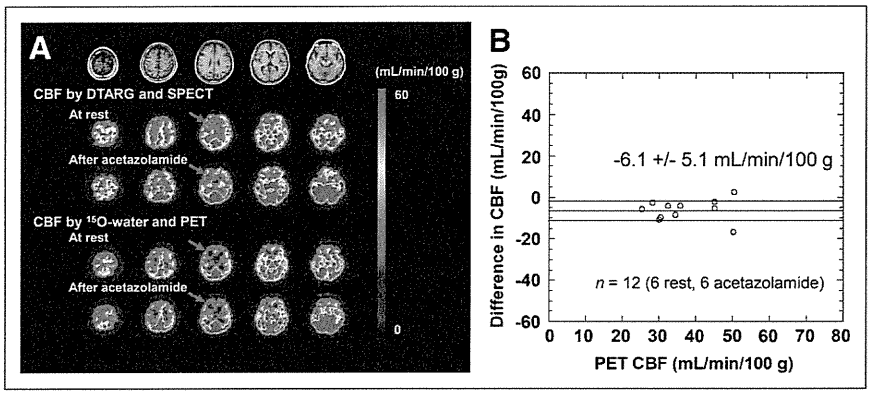

FIGURE 4. (A) MR and CBF images at rest and after acetazolamide stress assessed with corresponding measurements with ^{15}O-water PET (vs. PET evaluation) in patient with right internal carotid artery occlusion and left internal carotid stenosis. Gaussian filter was not applied to SPECT CBF in this display. (B) Bland–Altman plot. Moderate underestimation of CBF determined by DTARG method, compared with PET, is observed (mean difference, −6.1 mL/100 g/min). Correlation coefficient of $r = 0.88$ ($P < 0.001$) was found.

first injection when no vasodilating stress was given in 9 studies at 2 institutions (Fig. 5).

Quantitative CBF and CVR in response to acetazolamide challenge can be of significant prognostic value for patients considered for revascularization of cerebral arteries (*5–7*). The previously validated IMPARG method requires 2 independent scans on different days to assess the CVR (*5–7*), limiting it for routine clinical studies. The DTARG protocol to quantitatively assess CBF both at rest and after acetazolamide from a single dynamic SPECT session with the dual administration of ^{123}I-iodoamphetamine (*23*) facilitates clinical use. Errors caused by ambiguity in the absolute scaling, and possible changes in physiologic status of the subjects between scans, can be reduced substantially with the DTARG protocol. The quantitative reconstruction program enabled the compartment model–based kinetic analysis to compensate for the residual radioactivity concentration during the second session of the dynamic scan.

Major error sources in SPECT, namely attenuation and scatter, are only object-dependent (*14*) and not γ-camera– or collimator-dependent, and thus SPECT images obtained by this quantitative reconstruction package should be consistent across systems. Septal penetration of high-energy photons for ^{123}I is, however, collimator-dependent (*24*) but could be compensated as part of the TDCS scatter correction algorithm (*11*), as demonstrated in Supplemental Figure 2. The radioactivity concentration of the uniform cylinder phantom estimated in units of Bq/mL was consistent and showed variation within ±5.1% (Fig. 2; Supplemental Table 1), though a systematic underestimation by 12.5%, which is attributed to the BCFs being derived from a line source in air, reconstructed without scatter, attenuation, and septal penetration corrections. However, this underestimation does not affect the CBF estimation, because it relies on the direct cross-calibration between the γ-counter used to count the blood sample and the SPECT measurements.

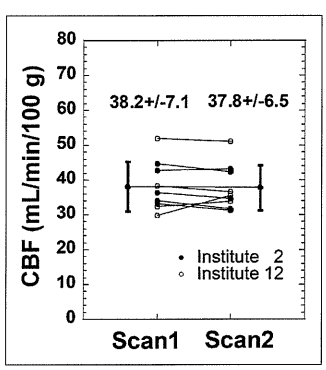

FIGURE 5. Results from rest–rest evaluation carried out at 2 institutions (2 and 12). In this study, DTARG method was performed as per normal protocol but without pharmacologic stress. CBFs estimated with first injection (left on graph) are in good agreement with those estimated after second injection (right on graph).

This phantom study also highlighted the importance of proper calibration and quality control of the γ-camera to avoid artifacts and bias in the reconstructed images. These corrections were applied, as for other clinical studies, by the vendors' software rather than as part of the QSPECT system, because these corrections are typically performed online and on-the-fly, with only the corrected data being stored. The nonuniformities seen on some phantom images should improve with more rigorous quality-control procedures.

The previously validated population-based input function requiring only a single arterial blood sample for scaling (*1,25–28*) has been incorporated in the software package. Blood from this single arterial sample is also used to measure arterial blood gases, which are relevant and of interest clinically in these patients. The timing of the single blood sample (~10 min after iodoamphetamine injection) was optimized previously (*1,25–28*) to minimize the errors associated with individual differences in shape of the arterial input function. In addition, absolute global CBF was estimated from SPECT images taken at an optimized mid scan time of approximately 30 min (24–28 min), rather than from the initial part of the study, to maximize the accuracy of using the population-based input function (*1,25–28*).

Partial-volume correction has not been implemented as part of this processing protocol. Partial-volume effects can potentially lead to underestimation of flow values in gray matter regions because of the limited resolution of SPECT. The small underestimation of 6.1 mL/100 g/min by the DTARG method, compared with ^{15}O-water PET (Fig. 4B), is attributed to the partial-volume effects due to differences in resolution between PET and SPECT. The underestimation can also lead to variations in CBF values obtained with different-

resolution collimators. However, consistent postreconstruction filtering, as applied in this study, can reduce this effect.

Only the reproducibility within an institution was assessed. Hence, the reproducibility of measurements between institutions cannot be gleaned from these data, particularly because patients with vascular disease were studied. Thus, unlike estimates from healthy volunteers, flow values and vascular reactivity are expected to vary from patient to patient, and flow values determined at one institution with one group of patients are therefore not directly comparable with flow values from another group of patients in another institution. A realistic brain phantom, such as recently developed by our group, simulating head contour with bone attenuation, could be used to assess the consistency of brain images between institutions.

CONCLUSION

The developed QSPECT package allows absolute CBF and CVR to be estimated in routine clinical studies. This multicenter study has demonstrated the applicability of QSPECT for a variety of clinical settings and equipment. Results from the studies suggest that a change of approximately 10% or 5 mL/min/100 g can be readily detected in follow-up studies. The graphical user interface for easily controlling the in-built sophisticated programs and tools ensures that routine use does not require dedicated support from scientific or computing staff. The package is now successfully used in over 130 institutions in Japan, and more than 25,000 patient studies have been analyzed with the QSPECT package.

ACKNOWLEDGMENTS

We thank the staff of each of the following institutions that participated in this project for their invaluable help with supporting the SPECT studies: Azabu Neurosurgical Hospital, Sapporo City; Asahikawa Red Cross Hospital, Asahikawa City; Handa City Hospital, Handa City; Ichinomiya Municipal Hospital, Ichinomiya City; Kashiwaba Neurosurgical Hospital, Sapporo City; Japanese Red Cross Kobe Hospital, Kobe City; Nakamura Memorial Hospital, Sapporo City; National Cardiovascular Center, Osaka; Ogori Daiichi General Hospital, Yamaguchi City; Oji General Hospital, Tomakomai City; Sunagawa City Medical Center, Sunagawa City; and Teine Keijinkai Hospital, Sapporo City. The present study was supported by the Japan Cardiovascular Research Foundation and a grant for Translational Research from the Ministry of Health, Labor and Welfare (MHLW), Japan.

REFERENCES

1. Iida H, Akutsu T, Endo K, et al. A multicenter validation of regional cerebral blood flow quantitation using [^{123}I]iodoamphetamine and single photon emission computed tomography. *J Cereb Blood Flow Metab.* 1996;16:781–793.
2. Hatazawa J, Iida H, Shimosegawa E, Sato T, Murakami M, Miura Y. Regional cerebral blood flow measurement with iodine-123-IMP autoradiography: normal values, reproducibility and sensitivity to hypoperfusion. *J Nucl Med.* 1997;38:1102–1108.
3. Yamaguchi T, Kanno I, Uemura K, et al. Reduction in regional cerebral metabolic rate of oxygen during human aging. *Stroke.* 1986;17:1220–1228.
4. Ogasawara K, Ito H, Sasoh M, et al. Quantitative measurement of regional cerebrovascular reactivity to acetazolamide using ^{123}I-*N*-isopropyl-*p*-iodoamphetamine autoradiography with SPECT: validation study using $H_2{}^{15}O$ with PET. *J Nucl Med.* 2003;44:520–525.
5. Ogasawara K, Ogawa A, Terasaki K, Shimizu H, Tominaga T, Yoshimoto T. Use of cerebrovascular reactivity in patients with symptomatic major cerebral artery occlusion to predict 5-year outcome: comparison of xenon-133 and iodine-123-IMP single-photon emission computed tomography. *J Cereb Blood Flow Metab.* 2002;22:1142–1148.
6. Ogasawara K, Ogawa A, Yoshimoto T. Cerebrovascular reactivity to acetazolamide and outcome in patients with symptomatic internal carotid or middle cerebral artery occlusion: a xenon-133 single-photon emission computed tomography study. *Stroke.* 2002;33:1857–1862.
7. Ogasawara K, Ogawa A. JET study (Japanese EC-IC Bypass Trial) [in Japanese]. *Nippon Rinsho.* 2006;64(suppl 7):524–527.
8. Fujita M, Ichise M, Zoghbi SS, et al. Widespread decrease of nicotinic acetylcholine receptors in Parkinson's disease. *Ann Neurol.* 2006;59:174–177.
9. Deloar HM, Watabe H, Kudomi N, Kim KM, Aoi T, Iida H. Dependency of energy and spatial distributions of photons on edge of object in brain SPECT. *Ann Nucl Med.* 2003;17:99–106.
10. Iida H, Eberl S, Kim KM, et al. Absolute quantitation of myocardial blood flow with ^{201}Tl and dynamic SPECT in canine: optimisation and validation of kinetic modelling. *Eur J Nucl Med Mol Imaging.* 2008;35:896–905.
11. Iida H, Eberl S. Quantitative assessment of regional myocardial blood flow with thallium-201 and SPECT. *J Nucl Cardiol.* 1998;5:313–331.
12. Eberl S, Chan HK, Daviskas E, Constable C, Young I. Aerosol deposition and clearance measurement: a novel technique using dynamic SPET. *Eur J Nucl Med.* 2001;28:1365–1372.
13. Hapdey S, Soret M, Ferrer L. Quantification in SPECT: myth or reality? A multicentric study. *IEEE Nucl Sci Symp Conf Rec.* 2004;5:3170–3317.
14. Graham LS, Fahey FH, Madsen MT, van Aswegen A, Yester MV. Quantitation of SPECT performance: report of Task Group 4, Nuclear Medicine Committee. *Med Phys.* 1995;22:401–409.
15. Hendel RC, Corbett JR, Cullom SJ, DePuey EG, Garcia EV, Bateman TM. The value and practice of attenuation correction for myocardial perfusion SPECT imaging: a joint position statement from the American Society of Nuclear Cardiology and the Society of Nuclear Medicine. *J Nucl Cardiol.* 2002;9:135–143.
16. Zaidi H, Koral KF. Scatter modelling and compensation in emission tomography. *Eur J Nucl Med Mol Imaging.* 2004;31:761–782.
17. Hudson HM, Larkin RS. Accelerated image reconstruction using ordered subsets of projection data. *IEEE Trans Med Imaging.* 1994;13:601–609.
18. Meikle SR, Hutton BF, Bailey DL. A transmission-dependent method for scatter correction in SPECT. *J Nucl Med.* 1994;35:360–367.
19. Iida H, Narita Y, Kado H, et al. Effects of scatter and attenuation correction on quantitative assessment of regional cerebral blood flow with SPECT. *J Nucl Med.* 1998;39:181–189.
20. Narita Y, Eberl S, Iida H, et al. Monte Carlo and experimental evaluation of accuracy and noise properties of two scatter correction methods for SPECT. *Phys Med Biol.* 1996;41:2481–2496.
21. Narita Y, Iida H, Eberl S, Nakamura T. Monte Carlo evaluation of accuracy and noise properties of two scatter correction methods for ^{201}Tl cardiac SPECT. *IEEE Trans Nucl Sci.* 1997;44:2465–2472.
22. Willowson K, Bailey DL, Baldock C. Quantitative SPECT reconstruction using CT-derived corrections. *Phys Med Biol.* 2008;53:3099–3112.
23. Kim K, Watabe H, Hayashi T, et al. Quantitative mapping of basal and vasareactive cerebral blood flow using split-dose ^{123}I-idoamphetamine and single photon emission computed tomography. *Neuroimage.* 2006;33:1126–1135.
24. Kim KM, Watabe H, Shidahara M, Ishida Y, Iida H. SPECT collimator dependency of scatter and validation of transmission dependent scatter compensation methodologies. *IEEE Trans Nucl Sci.* 2001;48:689–696.
25. Iida H, Itoh H, Nakazawa M, et al. Quantitative mapping of regional cerebral blood flow using iodine-123-IMP and SPECT. *J Nucl Med.* 1994;35:2019–2030.
26. Iida H, Nakazawa M, Uemura K. Quantitation of regional cerebral blood flow using 123I-IMP from a single SPECT scan and a single blood sampling: analysis on statistical error source and optimal scan time [in Japanese]. *Kaku Igaku.* 1995;32:263–270.
27. Kurisu R, Ogura T, Takikawa S, Saito H, Nakazawa M, Iida H. Estimation and optimization of the use of standard arterial input function for split-dose administration of *N*-isopropyl-*p*[^{123}I]iodoamphetamine [in Japanese]. *Kaku Igaku.* 2002;39:13–20.

28. Ogura T, Takikawa S, Saito H, Nakazawa M, Shidahara M, Iida H. Validation and optimization of the use of standardized arterial input function in *N*-isopropyl-*p*[^{123}I]iodoamphetamine cerebral blood flow SPECT [in Japanese]. *Kaku Igaku.* 1999;36:879–890.
29. Shidahara M, Watabe H, Kim KM, et al. Evaluation of a commercial PET tomograph-based system for the quantitative assessment of rCBF, rOEF and $rCMRO_2$ by using sequential administration of ^{15}O-labeled compounds. *Ann Nucl Med.* 2002;16:317–327.
30. Iida H, Higano S, Tomura N, et al. Evaluation of regional differences of tracer appearance time in cerebral tissues using [^{15}O] water and dynamic positron emission tomography. *J Cereb Blood Flow Metab.* 1988;8:285–288.
31. Iida H, Kanno I, Miura S, Murakami M, Takahashi K, Uemura K. Error analysis of a quantitative cerebral blood flow measurement using $H_2{}^{15}O$ autoradiography and positron emission tomography, with respect to the dispersion of the input function. *J Cereb Blood Flow Metab.* 1986;6:536–545.
32. Iida H, Kanno I, Miura S, Murakami M, Takahashi K, Uemura K. A determination of the regional brain/blood partition coefficient of water using dynamic positron emission tomography. *J Cereb Blood Flow Metab.* 1989;9:874–885.
33. Iida H, Shoji Y, Sugawara S, et al. Design and experimental validation of a quantitative myocardial ^{201}Tl SPECT System. *IEEE Trans Nucl Sci.* 1999;46:720–726.
34. Narita Y, Iida H. Scatter correction in myocardial thallium SPECT: needs for optimization of energy window settings in the energy window-based scatter correction techniques [in Japanese]. *Kaku Igaku.* 1999;36:83–90.
35. Eberl S, Kanno I, Fulton RR, Ryan A, Hutton BF, Fulham MJ. Automated interstudy image registration technique for SPECT and PET. *J Nucl Med.* 1996;37:137–145.